Probing silicate weathering reactions in soils with B isotopes

A. Voinot, M.-P. Turpault, S. Rihs, L. Mareschal, F. Chabaux, D. Lemarchand

Probing silicate weathering reactions in soils with B isotopes

Voinot A.[1, 2], M.-P.Turpault[1], S. Rihs[2], L. Mareschal[1, 3], F. Chabaux[2] and D. Lemarchand[2]

[1]Unité de Recherche Biogéochimie des Ecosystèmes Forestiers (INRA), F-54280 Champenoux

[2]Laboratoire d'Hydrologie et de Géochimie de Strasbourg, EOST-CNRS-UMR 7517, Université de Strasbourg, France

[3]CIRAD, UMR Eco&Sols, Ecologie Fonctionnelle & Biogéochimie des Sols & Agroécosystèmes (SupAgro-CIRAD-INRA-IRD), F-34060 Montpellier

Keywords

Boron isotopes, Breuil-Chenue, weathering, soil minerals

Abstract

The determination of the mechanisms and extent of soil mineral weathering can be challenging, and the caveats reside in 1) difficulty identifying minerals that are actually involved in weathering reactions, 2) non-stoichiometric release of cations during weathering processes due to coupled dissolution, precipitation and transformation reactions and, 3) impact of vegetation activity on elemental cycles in upper soil horizons.

To better characterize mechanisms controlling mineral weathering in soils and trace the evolution of B concentration and isotope ratios during chemical weathering, quantitative mineralogical analyses were coupled to B isotopes in a group of minerals (biotite, muscovite, K-feldspar and albite). Samples were selected along an Alocrisol (Alumic Cambisol, WRB FAO) soil profile from the bedrock (at 130 cm depth) up to 20 cm depth, developed on granitic bedrock in the Breuil-Chenue forest (France). The samples consist of residual primary minerals associated with weathering secondary phases (vermiculite, kaolinite…) in varying proportions.

The B isotopic compositions of the most pristine minerals span a very narrow range of values (around -31‰), whereas all secondary phases point to a much heavier value (around -16‰), regardless of mineralogy. Our results also show a mineral-dependent evolution of B concentration or isotopic composition as weathering progresses: no variation is observed during dissolution of K-feldspars; B behaves like a very mobile element in micas (biotite and muscovite), whereas it concentrates in weathered products derived from albite. However, rates of B concentrations and changes in isotopic compositions appear to be much faster than those inferred from mineralogy or major element concentrations determined by XRD and bulk chemical analyses, respectively. These results indicate that B is involved in very early weathering reactions and raises the question of its actual location in the structure of the various soil minerals as well as its pathway to solution.

1. Introduction

The generation of weathered particles and dissolved elements in soils and rivers is a complex process involving a combination of physicochemical and biological mechanisms. Usually, major or trace elements are used as proxies to assess the main parameters controlling weathering. These tracers have been used to determine weathering rates from soil profiles to continental scale watersheds (Augustin et al., 2016; Bastian et al., 2017; Maffre et al., 2018; Millot et al., 2002; Rasmussen et al., 2011; Riebe et al., 2017; Turner et al., 2010; Viers et al., 2009; Viville et al., 2012; White, 2008). Determining continental weathering fluxes based on elemental mass balances from soil solutions or river chemistry may often lead to ambiguous interpretation, especially under the influence of the biota (Ganor et al., 2009; Kelly et al., 1998; Maher and Navarre-Sitchler, 2019; Wild et al., 2019). Only in rare cases, when biological and lithological processes are spatially disconnected, can the distinction between bio-related mechanisms and water/rock interaction be made (White et al., 2005).

Boron behaves as a very incompatible element during magmatic processes (Tonarini et al., 2003) and is incorporated into silicate minerals in either trigonal or tetrahedral crystallographic sites (Anovitz and Grew, 1996). In phyllosilicates such as biotite, muscovite, smectite and illite, B is either located in tetrahedral sites in substitution for Si (Hålenius et al., 2010; Voinot et al., 2013; Williams and Hervig, 2005) or forms surface complexes on minerals and interlayer sites (Voinot et al., 2013; Williams et al., 2001). Boron can also substitute for aluminum in feldspar minerals, in trigonal sites in plagioclases (Geisinger et al., 1988; Icenhower et al., 2008; Martens et al., 2000) or tetrahedral sites in K-feldspars (Krzhizhanovskaya et al., 2012). The distribution of B isotopes between trigonal and tetrahedral sites is controlled by the crystallographic structure as well as the temperature of the fluid (Gaillardet and Lemarchand, 2018; Marschall et al., 2009; Sanchez-Valle et al., 2005; Tonarini et al., 2003). Therefore, the B isotopic composition of the various crystallographic sites within a same mineral can span a large range of values, with differences of about 40‰ observed between interlayer and

tetrahedral sites in illite-smectite interlayered minerals (Williams and Hervig, 2002) or up to 80‰ between interlayer and structural sites in biotite minerals (e.g., from the Bancroft ON, Canada pegmatite; Voinot *et al.* 2013). These intra-mineral heterogeneities give B the potential to be a suitable tracer of various weathering mechanisms such as phyllosilicate dissolution versus transformation (Voinot et al., 2013).

In this study, we analyzed the chemical composition as well as the B concentration and isotope ratios in a series of granite-forming minerals (biotite, muscovite, albite and K-feldspar) and their associated weathering products. Primary/secondary mineral assemblages were handpicked along a soil weathering profile. The main goal was to assess the evolution of B concentration and isotope ratios during chemical weathering of the most common granite-forming minerals, and to evaluate the potential of B as a proxy for silicate weathering reactions in soils.

2. Site and sampling

2.1. Site and soil

The Breuil-Chenue experimental forest site, created in 1976 by the INRA BEF team belongs to the ANAEE and SOERE F-ORE-T network. The site is located in the Morvan region (47°18’ N, 4°5’ E), in the northeastern part of Massif Central Mountains, on a plateau at an altitude of 638 m with a slight northwestern facing slope. The average yearly air temperature and precipitation are 9°C and 1280 mm, respectively. The bedrock comprises a two-micas granite, showing small variations in the size of the mineral grains, from 0.1 to 1 mm (Mareschal et al., 2015). The main mineral phases in the bedrock granite are quartz (34 to 35%), K-feldspar (23.8 to 24.2%), albite (30.3 to 31.2%), muscovite/white mica (8.1 to 8.9%), and biotite (1.2 to 2.2%) as well as some accessory minerals such as apatite and zircon (Mareschal et al., 2010; Mareschal et al., 2012). K-feldspar and some albite crystallized as perthite (Mareschal et al., 2015), and is referred to here as simply K-Feldspar.

Although this granite shows very few signs of hydrothermal alteration, some scattered evidence of later hydrothermal fluid circulation has been identified through precipitation of hematite as well as the destabilization of albite and biotite into white mica and chlorite, respectively (Mareschal, 2008; Mareschal et al., 2015). Signs of hydrothermal activity are more pronounced at the boundary with the underlying unit, where aplites and pegmatites have been described with increased presence of Sn and W-rich phases (cassiterite and scheelite, respectively), some 2 km to the southwest of the study site (Carrat, 1969; Mareschal, 2008).

The soil is classified as an Alocrisol (AFES, 1995) or Alumic Cambisol (WRB FAO) (Mareschal et al., 2010; Mareschal et al., 2012). Two main mineral transformation reactions have been identified in this soil: 1) transformation of micas (muscovite and biotite) to 2:1 and hydroxy-interlayered phyllosilicates (vermiculite or smectite) in the upper soil horizon (20-30 cm), and 2) destabilization of biotite and albite into kaolinite and gibbsite in the deeper soil horizons (>1 m) (Figure 1, Mareschal, 2008).

Chemical compositions of primary and associated weathering minerals have been determined in an earlier study via thin sections microprobe analysis at Lorraine University in Nancy (Mareschal, 2008). Results are reported in Table 1. The cationic exchange capacity (CEC) is very low in the lower soil horizon (2.7-5.8 $cmol.kg^{-1}$), but increases in the shallower horizon (9 $cmol.kg^{-1}$ at 0-5 cm) due to higher organic matter content. The pH of the soil solutions range from 5.0 in the 100-140 cm soil horizon down to 3.8 in the shallowest soil horizon (Mareschal, 2008).

2.2. Mineral separation

About 100 to 200 mg of primary granite-forming minerals (biotite, muscovite, albite and K-feldspar, Figure 1) were handpicked under a binocular microscope from bulk soil samples and from unaltered crushed bedrock. Quartz was not considered due to its very low B concentration (usually lower than 1 µg.g-1 , Anovitz and Grew, 1996; Christ, 1969; Yamaoka et al., 2012).

Each sample consists of a mixture of residual parent mineral and secondary/replacement phases that have precipitated within parent mineral as a result of dissolution or transformation. Because of the mineral separation procedure, possible traces of accessory minerals may remain in the handpicked mineral fraction.

Three unaltered granite samples (noted 1, 0a and 0b) were collected at three different locations within the sampling trench (30 m long, 1.4 m deep, Figure 1). The edges of the blocks were trimmed to remove the layer of regolith, and the remaining material was crushed into millimeter-sized grains before mineral separation. The bedrock exhibits traces of very localized hydrothermal alteration, with veins of quartz and hematite. Granite block #1 was collected at a depth of 0.8 to 1m in the soil (Figure 1) and shows evidence of weathering, such as precipitation of iron oxides in veins. Granite blocks #0a and #0b were sampled at a depth of about 1.4 m, at the interface between the bedrock and the soil, from which only biotite minerals were separated and analysed (samples B0a, B0b, Figure 1).

Samples were collected through the soil profile: 20-30 cm, as well as 110-120 cm, 120-130 cm and 130-140 cm, corresponding to the soil horizons B1 and C, respectively (Figure 1, Gontier et al., 2015 ; Mareschal et al., 2010). Soil sampling intervals were selected to target specific weathering reactions described in section 2.1. As such, only biotites were collected from the shallowest soil horizon (20-30 cm). Further, a distinction was made between coarse biotite grains (> 200 µm, separated from the 0.2-2 mm sieved bulk soil) and finer grains (50-200 µm) to assess the influence of grain size on B isotopes and weathering reactions. Biotite minerals were handpicked from the bulk soil matrix before being processed through a magnetic sector and vibrator (AA DYNA-MITE Electric vibrator 230V 50Hz, 10VA) for further separation from other mineral phases. Traces of accessory minerals were likely in the separated mineral phases, especially from those extracted from unaltered granite bedrock.

Of all albite samples, one sample collected between 1.3 and 1.4 m depth was showing mineralogical evidence of hydrothermal alteration (traces of hematite) and is hereafter referred to as AH.

2.3. Soil solution extraction

Pore and bound soil solutions were collected in soil horizons from which mineral samples were collected (20-30 cm and 120-140 cm, Figure 1). Water was extracted from the soil samples via centrifugation (Jouan KR422 centrifuge) using double-bottomed polycarbonate containers, precleaned with 0.5N HCl to minimize potential B contamination. Centrifugation was performed in two steps, starting with 20 min at 1000 rpm (acceleration of ≈ 180 G, pF = 3.25) followed by 20 min at 3000 rpm (≈ 2750 G, pF = 4.2) in order to extract pore and bound water, respectively (Turpault et al., 2005). A total volume of about 250 mL of water was extracted for each depth, corresponding to a mass of soil of ≈11 kg for the 20-30 cm horizon and ≈ 25 kg in the deepest horizon (Table 2). No pore water was extracted in the deepest soil horizon (120-140cm).

3. Analytical methods

3.1. Differential thermal analyses

Differential thermal analyses were used to directly quantify the amount of gibbsite and kaolinite in the samples. These analyses were conducted on about 10 mg of solid sample (Caner et al., 2011) using a TA Instrument SDT Q600 at the Laboratoire Hydrasa (Université de Poitiers). During the procedure, the temperature was gradually increased at a rate of 10°C/min from 25 to 1000°C, while precisely monitoring the mass of the sample (Kissinger, 1957). The mass loss between 250 and 285°C allows direct quantification of gibbsite from sample as follows:

$$X_{gibbsite} = \frac{\Delta_{wt-spl}}{\Delta_{wt-gibbsite}} \qquad \text{(eq. 1)}$$

where $X_{gibbsite}$ is the fraction of gibbsite in the solid sample, Δ_{wt-spl} and $\Delta_{wt-gibbsite}$ correspond to the relative weight loss between 250 and 285°C of the sample and the pure gibbsite, respectively ($\Delta_{wt-gibbsite}$= 31.2 %) (Dejou, 1977). Similarly, the relative amount of kaolinite can be determined from the relative mass loss between 440 and 550°C ($\Delta_{wt-kaolinite}$ = 13.6%) (Dejou, 1977).

3.2. X-ray diffraction

Identification of major mineral phases was performed by X-ray diffraction analyses on powdered samples at the Laboratoire de Biogéochimie des Ecosystèmes Forestiers (BEF, INRA, Champenoux) using a Siemens D5000 diffractometer fitted with a graphite monochromator with selected Cu-*K*α radiation (30 mA/40 kV). X-ray diffraction data were collected from 1.5° to 70.2° with a 0.01° increment and 6 seconds acquisition time. In order to distinguish chlorite from vermiculite and hydroxyl-interlayered-vermiculite in biotite samples, additional X-ray diffraction analyses were performed on K-saturated oriented samples heated at 110, 330, 440, 550 and 650°C. For these analyses, diffracted rays were collected from 2° to 20° with an increment of 0.01° and 3 seconds acquisition time.

3.3. Scanning electron microscopy

Scanning electron microscopy (SEM) was used to confirm the presence of mineral phases identified by X-ray diffraction. A Tescan Vega II microscope equipped with an Edax Pegasus X-ray analysis device was used at the Laboratoire d'Hydrogéologie et de Géochimie de Strasbourg (LHyGeS). Samples were deposited on glass slides and carbon coated. Both secondary electron and back-scattered electron detectors were used.

3.4. Major element concentrations

Samples were dried at 110°C before calcination at 1000°C to determine water content and loss on ignition, respectively. After alkaline fusion with lithium tetraborate, concentrations of major elements were determined by inductively coupled plasma atomic emission spectrometry (ICP-AES) and inductively-coupled plasma mass spectrometry (ICP-MS). Fifty (50) mg of calcinated samples were mixed with lithium tetraborate with a sample/flux ratio of 7.5 and placed in an oven under controlled Ar atmosphere at 1000°C for 30 minutes. The fusion residue was then dissolved in a nitric acid/glycerin solution (Besnus and Rouault, 1973; Samuel et al., 1985). The overall analytical uncertainty is < 3 % (±2σ) for major element concentrations.

3.5. Quantitative mineralogy

X-ray diffraction data (see annex Figure A1) and SEM observations were combined to identify significant mineral phases in each sample (Table 3). Based on differential thermal analyses, the contributions of kaolinite and gibbsite to the bulk chemical composition were subtracted, and the relative proportion of each remaining mineral phase was ascertained by solving the following system of equations, similarly to normative mineralogy of igneous rocks (Ezzaïm et al., 1999; Fichter et al., 1998a; Fichter et al., 1998b; Mareschal, 2008; Turpault, 2006):

$$\begin{cases} SiO_{2_{total}} = \sum X_i \times SiO_{2_i} \\ Al_2O_{3_{total}} = \sum X_i \times Al_2O_{3_i} \\ FeO_{total} = \sum X_i \times FeO_i \\ MgO_{total} = \sum X_i \times MgO_i \\ K_2O_{total} = \sum X_i \times K_2O_i \\ Na_2O_{total} = \sum X_i \times Na_2O_i \end{cases} \quad \text{(eq. 2)}$$

where $SiO_{2_{total}}$, $Al_2O_{3_{total}}$, FeO_{total}, MgO_{total}, K_2O_{total}, Na_2O_{total} refer to concentrations of different cations in the mineral assemblage; X_i is the mass fraction of the mineral *i* and SiO_{2_i}, $Al_2O_{3_i}$, FeO_i, MgO_i, K_2O_i, Na_2O_i correspond of the cation concentration in each mineral. The

composition of primary and secondary mineral phases (Table 1) and major element concentrations (Table 4) were used to solve the system of equations.

3.6. Boron concentrations and isotopic compositions

Boron was extracted from solid samples using K_2CO_3 alkaline fusion (Lemarchand et al., 2012). Fifty (50) mg of sample was analysed for both B concentration and isotopic composition. A 1:5 sample/flux ratio was used, and the mixture was placed in Pt-Au crucibles before heating at 950°C for 15 min in a muffle furnace (Cividini et al., 2010). Boron was then extracted from the fusion residue by 3 successive leaching steps using 1mL of ultra-pure water (Cividini et al., 2010). Boron concentrations were determined by Quadrupole ICPMS at LHyGeS on an aliquot of recovered leaching solution after a 10x dilution (Lemarchand et al., 2012). The long-term reproducibility of the method is 6% (±2SD).

Following a chemical purification using the B-specific resin Amberlite IRA-743 (Voinot et al., 2013), B isotopic compositions were subsequently determined by multi-collector ICP-MS (Thermo-Finnigan Neptune). The total procedural contamination is about 15 ng B and originates primarily from the muffle furnace and flux (Prigent et al., 2018). This contamination typically represents less than a few percents of the total B analysed and has a B isotopic composition (about -10 ‰) that is close to some of the samples that were measured, thus leading to limited potential isotopic shift. Boron isotopic compositions are expressed as the deviation in ‰-units from the NIST SRM 951 B isotopes standard processed though the same procedure as the samples:

$$R = \left(\frac{{}^{11}B/{}^{10}B_{sample}}{{}^{11}B/{}^{10}B_{standard}} - 1 \right) \times 1000 \qquad \text{(eq. 3)}$$

The long-term reproducibility of the entire B isotope analysis procedure is 0.6 ‰ (±2σ, n = 19)

224 (Cividini et al., 2010; Lemarchand et al., 2012). Chemical compositions (major elements) as well as B
225 concentrations and isotopic compositions of the samples are reported in Table 4.

226

227 4. Results

228 The mineral phases identified by XRD and SEM in each sample are reported in Table 3. Results from
229 the quantitative mineralogy calculations, as well as B concentrations and isotopic compositions are
230 illustrated in Figures 2 and 3, respectively. Results for the differential thermal and X-ray diffraction
231 analyses are provided in annex Figures A1 and A2.

232 4.1. K-feldspar

233 The combination of XRD, chemical and differential thermal analyses show no evidence of secondary
234 phases in K-feldspar samples (Figures 2 and A1, Table 3). Although chemical analyses of K-feldspars
235 show slight increase of the Na_2O/K_2O ratio with depth, suggesting a preferential dissolution of the
236 albite end-member, both B concentrations and isotopic compositions in handpicked K-feldspars
237 remain relatively constant along the soil profile, from 6.2 to 11.6 $\mu g.g^{-1}$ and -33.2 to -30.3 ‰,
238 respectively (Figure 3a).

239 4.2. Muscovite

240 Chemical, XRD and SEM analyses show no evidence of weathering of the muscovite. Traces of K-
241 Feldspar and quartz are found in muscovite samples (Figure 2) and are the result of the mineral
242 separation procedure. In contrast to the apparent lack of alteration and secondary mineral phases of
243 the handpicked muscovite samples, B concentrations and $\delta^{11}B$ values cover a relatively large range of
244 values, from 22.5 to 89.5 $\mu g.g^{-1}$ and from -30.7 to -19.4 ‰, respectively (Figure 3b). Samples M1, M2
245 and M3 show variable $\delta^{11}B$ values, ranging from -30.7 to -21.4‰, but have similar relatively high - B

246 concentrations between 76.1 and 89.5 $\mu g.g^{-1}$. The muscovite sample picked at the shallowest depth
247 (M4) shows the lowest B concentration at 22.5 $\mu g.g^{-1}$ and the highest $\delta^{11}B$ value (-19.4 ‰).

248 ### 4.3. Biotite

249 Quantitative mineralogy calculations performed on biotite collected in the deeper soil horizons (B1,
250 B2, B3 and B4) exhibit a gradual decrease of the proportion of biotite with decreasing depth, from 90
251 to 60 %, while vermiculite and kaolinite proportions increase at shallower depths (Figure 2).

252 Overall, B concentrations in biotite samples cover a large range of values from 0.9 to 80 $\mu g.g^{-1}$ and
253 tend to decrease as the proportion of secondary phases increases. In parallel, $\delta^{11}B$ values increase
254 with the proportion of secondary phases, from about -30‰ in the non-weathered biotite to about -
255 16 ‰ in the most weathered samples (Figures 2 and 3c). Biotite samples picked from unaltered
256 granite (samples B0a and B0b) exhibit variable B concentrations (21 and 74 $\mu g.g^{-1}$, respectively) and
257 $\delta^{11}B$ values (-31.1 ‰ and -26.8 ‰, respectively) but show small variations in their mineralogical
258 composition (Figures 2 and 3c).

259 In the shallowest soil horizon (20-30 cm), the coarse-grained biotite (B5a, B5b, > 200 µm) shows
260 mineralogical compositions that are intermediate between those from non-weathered granite (B0a
261 and B0b) and the biotite samples picked in the deeper soil horizons (B2 and B3), with small amounts
262 of vermiculite and kaolinite and high proportion of biotite (>60 %) (Figure 2). Samples B5a and B5b
263 also contain small amounts of chlorite, and exhibit slightly higher isotopic compositions (-23.5 and -
264 23‰, respectively) together with higher B concentrations (up to 80 $\mu g.g^{-1}$) than biotite sampled in
265 unaltered granite.

266 Finer grained samples collected from the same soil horizon (20-30cm, 50-200 µm fraction) are more
267 weathered and exhibit much lower amounts of residual parent biotite - between 19 % and 26 % for

samples B6b and B6a, respectively - associated with higher proportions of vermiculite (32-33 %) and kaolinite (around 24-25 %).

All samples contain approximately 10% quartz, including biotite grains sampled within the granite (samples B0a, B0b and B1), and likely result from the mineral separation process. Traces of Ti oxides (around 1 to 2 % in most samples) are also found, as well as up to 0.8% chlorite in samples B0b, B5a, B5b and B6a, with no direct correlation with B concentration or isotopic composition.

4.4. Albite

Albite picked from seemingly pristine looking granite (A1) contains about 15%. In albite collected within the saprolite (samples A2, A3 and A4), the parent albite minerals have almost entirely been replaced with kaolinite. SEM analyses of sample A2 (130 - 140 cm) reveal a highly altered sponge-like structure (Figure 4) composed primarily of kaolinite, with only traces of residual albite.

Traces of quartz, muscovite as well as traces of gibbsite (< 2 %) are found in all albite samples. Sample AH contain a significant amount of hematite (about 3%) likely resulting from hydrothermal alteration.

In contrast to biotite, B concentrations increase in weathered albite when $\delta^{11}B$ values increase from -24.7 ‰ (A1) to -15.4 ‰ (A4). Compared with other albite samples, sample AH, shows evidence of hydrothermal alteration, and is characterized by a much higher B concentration (472 $\mu g.g^{-1}$) and a lower B isotopic composition (-27.9 ‰).

4.5. Soil solutions

The extraction method used doesn't access water trapped within the phyllosilicate interlayers. Accessing this water would require a specific technique such as ion exchange, followed by neutron diffraction (OECD, 2000; Powell et al., 1997; Skipper et al., 1991). Pore waters could only be collected

290 from the uppermost soil layer (20-30 cm), as deeper soil samples from the 110 – 140 cm horizon
291 were dry. Boron concentration and isotopic composition of shallow pore waters are 12 ng.mL^{-1} and
292 +30.3 ‰, respectively (Table 2). The shallow bound water shows a slightly lower B concentration (8.4
293 ng.mL^{-1}) and lower B isotopic composition (+22.3 ‰). The deeper bound water (110-140 cm) is
294 characterized by a higher B concentration (12.5 ng.mL^{-1}) and slightly lower B isotopic composition
295 (+18.9 ‰).

296 # 5. Discussion

297 ## 5.1. Influence of sorting residues

298 Most samples contain between 0 and 20 % of accessory minerals, that couldn't be separated during
299 the mineral selection process. These include: quartz in biotite and albite, K-feldspar in muscovite and
300 muscovite in albite (except for albite sample AH which exhibits a quartz proportion of about 35%,
301 Figure 2). These are hereafter referred to as sorting residues.

302 Given that quartz in granitic rocks is usually characterized by very low B concentrations below 1 µg.g^{-1}
303 (Anovitz and Grew, 1996; Christ, 1969; Yamaoka et al., 2012), the presence of quartz in the samples
304 only affects B concentration through dilution, but is not expected to impact the δ^{11}B value. K-feldspar
305 samples don't show any evidence of accessory minerals and can therefore be considered as pure.
306 Traces of K-feldspar are found in muscovite samples (< 5%), with the exception of sample M2 where
307 the K-feldspar proportion is about 20%. Because B concentration and isotope ratios in K-feldspar
308 span a narrow range of values (from 6.2 to 11.6 µg.g^{-1} and -33.2 to -30.3 ‰, respectively), it's
309 possible to correct the sample concentration and isotopic composition from the contribution of the
310 K-feldspar sorting residue. Only the B concentration in sample M2 is affected beyond analytical
311 errors by the presence K-feldspar, and a corrected M2 concentration of about 64 µg.g^{-1} is therefore
312 reported in Figure 3b (sample M2*). All biotite samples contain about 10 to 15% quartz, thus leading

313 to a slight underestimation of their B concentrations but no impact on B isotope compositions. In
314 albite samples, contribution of the traces of muscovite on the bulk B budget is less than 12 $\mu g.g^{-1}$,
315 which represents 7.5 to 15% of the total analyzed B. Given the range of $\delta^{11}B$ values measured in the
316 various muscovite (from -30.7‰ to -19.4‰) and albite samples (-31.1‰ to -16.1‰), the expected
317 maximum shift in B isotope values resulting from muscovite traces in albite samples is less than 2.2
318 ‰. This contribution is not negligible and is greater than the analytical precision (about 0.6‰) but
319 remains small compared to the observed range of B isotopes variation in albite samples (≈ 15 ‰).

320 ## 5.2. Boron in primary non-weathered minerals

321 With the exception of albite sampled in seemingly unaltered granite (A1), which shows evidence of
322 early weathering (presence of kaolinite), all $\delta^{11}B$ values in non-weathered minerals span a very
323 narrow range of values at -31 ± 3‰ (Figure 3). These values are lower than the continental crust
324 inferred from B isotope analyses in tourmaline (-7 ‰, Chaussidon and Albarède, 1992) but are
325 consistent with published analyses of soil profiles developed on granite bedrock, like values from the
326 Strengbach catchment (Cividini et al., 2010; Lemarchand et al., 2012) or the Guyana Shield (Spivack
327 et al., 1987). These low values suggest cogenetic minerals in plutonic rocks have similar $\delta^{11}B$ values.
328 This is probably a result of the relatively small B isotopic fractionation coefficient (α = 1.005)
329 observed during crystallisation of silicate melts, as well as to the fact that B occupies similar
330 crystallographic sites in silicate minerals, substituting for Si or Al (Marschall et al., 2009; Tonarini et
331 al., 2003). Biotite samples that show no chemical or mineralogical evidence of alteration (B0a, B0b)
332 exhibit a significantly larger range of B concentrations (21 to 74 $\mu g.g^{-1}$) and $\delta^{11}B$ values (-26.8‰ to -
333 31.1‰). Sample B0a shows a $\delta^{11}B$ value similar to unaltered muscovite and K-feldspar samples, while
334 sample B0b shows higher B concentration with a $\delta^{11}B$ value similar to sample AH.

335 Samples B0b, B5a and AH have similar $\delta^{11}B$ values, ranging from -27.9 to -23.5‰ (Figures 3c and 3d).
336 In addition, the biotite samples B0b and B5a contain traces of chlorite (about 0.4%) and sample AH

337 contains traces of hematite. This seems to point towards a potential hydrothermal or supergene
338 alteration fluid imprint on B isotopic composition, as chlorite and hematite have been identified as
339 indicators of hydrothermal fluid interaction in the study site (Mareschal, 2008). High B
340 concentrations reaching several hundreds of $\mu g.mL^{-1}$ have been observed in hydrothermal fluids, and
341 exchange of B between host minerals and hydrothermal fluids is possible (Aggarwal and Palmer,
342 1995; Boschi et al., 2008; Yamaoka et al., 2015; Zeng et al., 2013).

343 ### 5.3. Boron in weathered minerals

344 Samples showing the highest proportions of secondary minerals (biotite B6a, B6b, B3, B4, and albite
345 A2, A3, A4, Figures 2 and 5) have similar $\delta^{11}B$ values around -18.5‰ ± 1.5‰. Sample M4 exhibits a
346 similar $\delta^{11}B$ value, yet exhibits no chemical and XRD evidence of mineralogical alteration.

347 Possible explanations for this homogeneous B isotopic composition in all weathered minerals may
348 involve either 1) B exchange between pore waters and all phases found in the mineral habits, which
349 has been observed in high temperature systems but not at surface conditions (Bobos and Williams,
350 2017; Clauer et al., 2018; Tonarini et al., 2003); 2) a preferential release of B from different
351 crystallographic sites (*i.e.,* structural or water-accessible sites), each characterized by distinct $\delta^{11}B$
352 signatures (Voinot et al., 2013; Williams et al., 2001) or 3) a difference in the weathering rate of at
353 least two generations of parent minerals characterized by distinct $\delta^{11}B$ values.

354 All weathered minerals span a very restricted range of $\delta^{11}B$ values despite the large variety of mineral
355 phases observed, with varying amounts of primary mineral residues associated with secondary
356 minerals like vermiculite, kaolinite or gibbsite (Figure 5). A common $\delta^{11}B$ signature in different
357 minerals suggests similar mechanisms controlling the incorporation of B into mineral weathering
358 products. The observed isotopic fractionation ($\Delta^{11}B_{solid\text{-}solution}$) is therefore not mineral specific, but
359 instead reflects similar crystallographic environment, with ^{10}B enriched tetrahedral $B(OH)_4^-$ being

preferentially adsorbed onto the mineral surfaces (Gaillardet and Lemarchand, 2018; Lemarchand et al., 2007; Muttik et al., 2011; Spivack et al., 1987; Williams et al., 2001).

Considering that trapped pore water have a $\delta^{11}B$ value around +20‰ (Table 2), and that the typical B isotopic fractionation generally observed between solids and solution at low temperature ($\Delta_{solid\text{-}solution}$) is close to -35‰ (Gaillardet and Lemarchand, 2018; Lemarchand et al., 2012 and discussion therein; Lemarchand et al., 2007; Muttik et al., 2011; Spivack et al., 1987), minerals in isotopic equilibrium with the pore water would have $\delta^{11}B$ values close to -15‰, consistent with minerals analyzed in this study. Similar observations were made on the evolution of B in the clay-size fractions collected from the Strengbach watershed (Lemarchand et al., 2012). However, the pore water value measured in this study only is a snapshot of the hydrogeochemical conditions at a given instant in time (July 2012), that can't be extrapolated to the several thousands of years required for the soil to develop (Moore and Singer, 1990; Stevens and Walker, 1970).

Interestingly, some samples show only minor changes in their mineralogical and chemical composition (muscovite samples M2, M3 and M4), yet exhibit $\delta^{11}B$ values similar to those observed in the most weathered products ($\delta^{11}B \approx$ -16 ‰ for sample M4) (Figures 2 and 5). This observation infers a large proportion of B in the bulk mineral can potentially exchange with the surrounding environment without evidence of alteration of mineralogical or crystallographic properties. Thus, a large proportion of B in these minerals is in exchangeable sites, such as reactive surfaces like those found in the interlayers, grain boudaries or crystal defects. The transfer of B to solution appears much faster than major elements, which is in agreement with previous laboratory dissolution experiments (Voinot et al., 2013; Williams et al., 2001). In both micas, the relatively rapid transfer of B without destruction of the crystal structure, as demonstrated by XRD analyses, may likely be facilitated by interfoliar spaces. The present study cannot firmly identify the exact mechanism(s) controlling B isotopic evolution during weathering of micas (surface interactions or structural breakdown of B-bearing sites). Further investigations at the crystallographic scale should help answer

this question. But it's clear that B behaves like a very mobile element during the weathering of micas, similarly to what has been observed in laboratory studies (Voinot et al., 2013; Williams and Hervig, 2002). While facilitated matter transport is expected in phyllosilicates where interfoliar spaces can be efficient water pathways, it challenges our understanding of water and element transport across a crystallized lattice as found in albite.

5.4. Boron: a proxy of weathering regime?

The similarity in B isotopic composition between cogenetic silicate minerals can potentially be used to trace the source(s) of parent materials as well as to give information about the weathering regime, provided that 1) the signature of unaltered parent material can be recovered from samples and 2) there is an observable difference between the B isotopic composition of weathered products and parent minerals. This difference can be magnified by two conditions: 1) in systems dominated by dissolution reactions leading to a relatively small rate of B incorporation into secondary phases, and 2) in systems where vegetation cover, which represents an isotopically fractionated B pool, is dense enough to control the B isotopic composition of solutions which precipitate secondary products (e.g. Cividini et al. 2010).

From this study, analyses of B isotopes in K-feldspar demonstrate that their dissolution in soils occurs without observable isotopic fractionation. The B isotopic composition of these minerals therefore remains unchanged during the development of the weathering profile and can be potentially used as a reference to compare against weathering products. Similarly, the homogeneity of B isotopic compositions observed in different weathering products reflects the signature of the local weathering regime, which can be described as the ratio between dissolution and precipitation rates, including a potential contribution of organic matter and atmospheric B inputs. The results of this study therefore indicate that the comparison of B isotopes between pristine primary minerals (i.e. K-feldspars) and secondary products (*i.e.,* clay minerals) could potentially be used in various natural

409 environments to resolve processes of source mixing and secondary mineral formation or
410 transformation of primary mineral phases, similarly to what has been shown in laboratory
411 experiments (Voinot et al., 2013) or observed in natural systems (Ercolani et al., 2019).

412 The results herein also demonstrate that the discrepancy between the evolution of the mineral
413 assemblage (inferred from X-ray diffraction and major element composition) and B isotopes is
414 mineral dependent (Figures 5 and 6). This property can potentially be used to determine the extent
415 of weathering reactions with more refinement than major element or traditional mineralogical
416 methods, or to identify the earliest stages of weathering reactions in soils. For example, if the $\delta^{11}B$
417 values measured in biotite minerals are close to the ones measured in muscovites and in K-Feldspars,
418 this would indicate a very early stage of weathering. In other cases, the progression of the
419 weathering reactions would differentially affect each mineral assemblage (Figures 5 and 6).

420 Boron concentration variations in weathered albite crystals differ from micas. Almost all albite
421 crystals show a near complete loss of the primary albite form by kaolinite mass (about 75%).
422 However, contrary to what can be observed in micas, the B concentration progressively increases
423 with the extent of weathering of the parent material, reaching up to 185 $\mu g.g^{-1}$, about twice the value
424 of the least weathered albite sample A1. Such an increase of the B concentration together with the
425 evolution of B isotopes may be explained by two different processes:

426 1) the presence of a low-solubility B-rich phase with a B isotopic composition close to -15‰ that
427 progressively controls the B mass balance as the weathering reaction progresses. In order to explain
428 B behaviour in all the samples, this accessory phase should be found in both micas and albite but not
429 in K-feldspar. This phase should only be found at trace level in micas, as the B concentration in
430 weathered products almost decreases to the analytical detection limit, but be in much larger
431 proportion in albite to explain the increase in B concentration. Tourmaline might be a potential
432 candidate for such an accessory mineral phase, but it has not been observed in our samples and so
433 far, none of our observations can support this hypothesis.

2) the development of a very large reactive water/rock interface allowing a large amount of B to be incorporated in secondary products. Like other elements, such as U and Mo, specific chemical conditions can lead to very strong affinity with clay minerals and can show adsorbed concentrations of several hundreds of $\mu g.g^{-1}$ (Davey and Scott, 1956; Li et al., 2012; Sikalidis et al., 1989; Tournassat et al., 2018; Xu et al., 2013). It may be hypothesized that the development of a very small and dense porous network as the albite minerals are being weathered could generate such a large reactive surface. This hypothesis is supported by SEM analyses of the weathered albite samples (Figure 4) that clearly show a sponge-like porous structure. This is a well-known evolution of albite minerals for which the surface of water-rock interaction can increase by a factor of two during weathering (White et al., 2001). Similar to the B-specific resin (Amberlite IRA 743), where the spongy structure leads to apparent huge partitioning coefficient (Lemarchand et al., 2002), it can be hypothesized that the formation or activation of nano-channels may considerably increase the reactive surface of the mineral and lead to an accumulation of B in the weathered albite product. This hypothesis, which seems to best fit our data, also points to a very different description of the weathering reactions than those used in classic numerical models. Precipitation of secondary products would not be controlled by supersaturation of the bulk solution with respect to secondary phases after dissolution of the primary ones, but would be controlled by the mineralogy of the mineral parent. For biotite, the low B concentration would indicate an efficient transport of water, thus draining mobile elements. For albite, the development of a nano- to micro-porous network would drastically increase the reactive surface while slowing down the velocity of water (high porosity, but low permeability), thus leading to an enhanced incorporation of soluble elements.

6. Conclusion

Investigation of B concentration and isotopic composition in weathered silicate minerals (biotite, muscovite, albite and K-feldspar) with associated secondary phases (gibbsite, kaolinite, vermiculite) clearly emphasizes B sensitivity to water-rock processes. The homogenous B isotopic signature in the

initial primary minerals on one hand and secondary weathering products on the other can greatly help understanding weathering conditions. In particular, combining B isotope analyses in minerals with varying weathering rates could help identify the primary mineral source of B and bring quantitative information on the soil forming mechanisms.

Among the minerals analyzed in this study, combined analyses of K-feldspar and muscovite minerals appear to be an ideal way to investigate weathering processes in soils, as these minerals show contrasted B behaviour while still showing little to no mineralogical change with weathering, thus limiting complicated interpretations caused by presence of secondary phases. The second advance made by this study is to recognize different B behaviour during weathering, indicating distinct weathering mechanisms. B appears to behave like a very mobile element in micas from a chemical point of view but accumulates in the weathering products of albite.

This study points to unresolved questions that require further investigations. In particular, it remains unclear if the B isotopic composition of secondary phases reflects isotopic equilibrium with the surrounding solution or a preferential disruption of specific B-bearing sites. In addition, B shows a very high mobility B in minerals showing no evidence of crystallographic transformation.

Once the mechanisms controlling the B distribution in weathered silicate minerals will be better understood, combined B analyses in soil or rivers detrital mineral grains would certainly provide strong information on weathering controls and help understanding sedimentary records.

Acknowledgements

This work was supported by the INSU French National funding program (EC2CO, Cycles hydro-biogéochimiques, Transferts et Impacts écotoXicologiques, CYTRIX) and funding coming from both Alsace and Lorraine regions. The ISOSIL ANR, thanks to Nathalie Vigier, has provided funding to support mineral sorting from bulk soil matrices as well as rock grinding (done by Bruno Simon).

483 We would also like to thank A. Legout (Breuil forest site scientific supervisor) and C. Calvaruso for
484 the help with the soil sampling, and K. Durocher for the manuscript proofreading.

485

486

487

7. References

Aggarwal, J.K. and Palmer, M.R. (1995) Fractionation of boron isotopes in Icelandic hydrothermal systems. University of Auckland, New Zealand.

Anovitz, L.M. and Grew, E.S. (1996) Mineralogy, petrology and geochemistry of boron; an introduction. Reviews in Mineralogy and Geochemistry 33, 1-40.

Augustin, F., Houle, D., Gagnon, C. and Courchesne, F. (2016) Evaluation of three methods for estimating the weathering rates of base cations in forested catchments. CATENA 144, 1-10.

Bastian, L., Revel, M., Bayon, G., Dufour, A. and Vigier, N. (2017) Abrupt response of chemical weathering to Late Quaternary hydroclimate changes in northeast Africa. Scientific Reports 7, 44231.

Besnus, Y. and Rouault, R. (1973) Une methode d'analyse des roches au spectrometre d'arc à lecture directe par un dispositif d'électrode rotative. Analusis 2, 111-116.

Bobos, I. and Williams, L.B. (2017) Boron, lithium and nitrogen isotope geochemistry of NH4-illite clays in the fossil hydrothermal system of Harghita Bãi, East Carpathians, Romania. Chemical Geology 473, 22-39.

Boschi, C., Dini, A., L. Früh-Green, G., Zandomeneghi, G., Kelley, D. and Meier, B. (2008) Boron isotope systematic of marine hydrothermal fluids: New insights from the Lost City Hydrothermal System (MAR 30°N).

Caner, L., Petit, S., Joussein, E., Fritsch, E. and Herbillon, A.J. (2011) Accumulation of organo-metallic complexes in laterites and the formation of Aluandic Andosols in the Nilgiri Hills (southern India): similarities and differences with Umbric Podzols. European Journal of Soil Science 62, 754-764.

Carrat, H.G. (1969) Evolution de la granitisation et du volcanisme dans le Morvan. Bulletin de la Société Géologique de France S7-XI, 574-587.

Chaussidon, M. and Albarède, F. (1992) Secular boron isotope variations in the continental crust: an ion microprobe study. Earth and Planetary Science Letters 108, 229-241.

Christ, C.L.a.H.H. (1969) Handbook of Geochemistry Chapter 5 - Boron. Springer-Verlag, Berlin, Heidelberg.

Cividini, D., Lemarchand, D., Chabaux, F., Boutin, R. and Pierret, M.C. (2010) From biological to lithological control of the B geochemical cycle in a forest watershed (Strengbach, Vosges). Geochimica et Cosmochimica Acta 74, 3143-3163.

Clauer, N., Williams, L.B., Lemarchand, D., Florian, P. and Honty, M. (2018) Illitization decrypted by B and Li isotope geochemistry of nanometer-sized illite crystals from bentonite beds, East Slovak Basin. Chemical Geology 477, 177-194.

Davey, P.T. and Scott, T.R. (1956) Adsorption of Uranium on Clay Minerals. Nature 178, 1195.

Dejou, J. (1977) Évolution superficielle des roches cristallines et cristallophylliennes dans les régions tempérées. INRA, Paris :.

Ercolani, C., Lemarchand, D. and Dosseto, A. (2019) Insights on catchment-wide weathering regimes from boron isotopes in riverine material. Geochimica et Cosmochimica Acta 261, 35-55.

Ezzaïm, A., Turpault, M.P. and Ranger, J. (1999) Quantification of weathering processes in an acid brown soil developed from tuff (Beaujolais, France) Part II. Soil formation. Geoderma 87, 155-177.

Fichter, J., Bonnaud, P., Turpault, M.-P. and Ranger, J. (1998a) Quantitative determination of minerals in acid forest soils of granite. Zeitschrift für Pflanzenernährung und Bodenkunde 161, 129-139.

Fichter, J., Turpault, M.-P., Dambrine, E. and Ranger, J. (1998b) Mineral evolution of acid forest soils in the Strengbach catchment (Vosges mountains, N-E France). Geoderma 82, 315-340.

Gaillardet, J. and Lemarchand, D. (2018) Boron in the Weathering Environment, in: Marschall, H., Foster, G. (Eds.), Boron Isotopes: The Fifth Element. Springer International Publishing, Cham, pp. 163-188.

Ganor, J., Reznik, I.J. and Rosenberg, Y.O. (2009) Organics in Water-Rock Interactions. Reviews in Mineralogy and Geochemistry 70, 259-369.

537 Geisinger, K.L., Oestrike, R., Navrotsky, A., Turner, G.L. and Kirkpatrick, R.J. (1988) Thermochemistry
538 and structure of glasses along the join NaAlSi3O8-NaBSi3O8. Geochimica et Cosmochimica Acta 52,
539 2405-2414.
540 Gontier, A., Rihs, S., Chabaux, F., Lemarchand, D., Pelt, E. and Turpault, M.-P. (2015) Lack of bedrock
541 grain size influence on the soil production rate. Geochimica et Cosmochimica Acta 166, 146-164.
542 Hålenius, U., Skogby, H., Edén, M., Nazzareni, S., Kristiansson, P. and Resmark, J. (2010) Coordination
543 of boron in nominally boron-free rock forming silicates: Evidence for incorporation of BO3 groups in
544 clinopyroxene. Geochimica et Cosmochimica Acta 74, 5672-5679.
545 Icenhower, J.P., McGrail, B.P., Shaw, W.J., Pierce, E.M., Nachimuthu, P., Shuh, D.K., Rodriguez, E.A.
546 and Steele, J.L. (2008) Experimentally determined dissolution kinetics of Na-rich borosilicate glass at
547 far from equilibrium conditions: Implications for Transition State Theory. Geochimica et
548 Cosmochimica Acta 72, 2767-2788.
549 Kelly, E.F., Chadwick, O.A. and Hilinski, T.E. (1998) The Effect of Plants on Mineral Weathering.
550 Biogeochemistry 42, 21-53.
551 Kissinger, H.E. (1957) Reaction Kinetics in Differential Thermal Analysis. Analytical Chemistry 29,
552 1702-1706.
553 Krzhizhanovskaya, M.G., Bubnova, R.S., Depmeier, W., Rahmoun, N.-S., Filatov, S.K. and Ugolkov, V.L.
554 (2012) A new borosilicate feldspar, KBSi3O8: synthesis, crystal structure and thermal behavior.
555 Zeitschrift f√ºr Kristallographie - Crystalline Materials 227, 446-451.
556 Lemarchand, D., Cividini, D., Turpault, M.P. and Chabaux, F. (2012) Boron isotopes in different grain
557 size fractions: Exploring past and present water,Äìrock interactions from two soil profiles
558 (Strengbach, Vosges Mountains). Geochimica et Cosmochimica Acta 98, 78-93.
559 Lemarchand, D., Gaillardet, J., Göpel, C. and Manhès, G. (2002) An optimized procedure for boron
560 separation and mass spectrometry analysis for river samples. Chemical Geology 182, 323-334.
561 Lemarchand, E., Schott, J. and Gaillardet, J. (2007) How surface complexes impact boron isotope
562 fractionation: Evidence from Fe and Mn oxides sorption experiments. Earth and Planetary Science
563 Letters 260, 277-296.
564 Li, S.Y., Xie, S.B., Zhao, C., Liu, J.X., Ling, H. and Gu, Z.H. (2012) Study on Adsorption of Uranium in
565 Wastewater by Clay. Applied Mechanics and Materials 209-211, 2081-2085.
566 Maffre, P., Ladant, J.-B., Moquet, J.-S., Carretier, S., Labat, D. and Goddéris, Y. (2018) Mountain
567 ranges, climate and weathering. Do orogens strengthen or weaken the silicate weathering carbon
568 sink? Earth and Planetary Science Letters 493, 174-185.
569 Maher, K. and Navarre-Sitchler, A. (2019) Reactive Transport Processes that Drive Chemical
570 Weathering: From Making Space for Water to Dismantling Continents. Reviews in Mineralogy and
571 Geochemistry 85, 349-380.
572 Mareschal, L. (2008) Effet des substitutions d'essences forestières sur l'évolution des sols et de leur
573 minéralogie : bilan après 28 ans dans le site expérimental de Breuil (Morvan). Ph.D. thesis of Nancy
574 University, France.
575 Mareschal, L., Bonnaud, P., Turpault, M.P. and Ranger, J. (2010) Impact of common European tree
576 species on the chemical and physicochemical properties of fine earth: An unusual pattern. European
577 Journal of Soil Science 61, 14-23.
578 Mareschal, L., Turpault, M.P., Bonnaud, P. and Ranger, J. (2012) Relationship between the
579 weathering of clay minerals and the nitrification rate: a rapid tree species effect. Biogeochemistry, 1-
580 17.
581 Mareschal, L., Turpault, M.P. and Ranger, J. (2015) Effect of granite crystal grain size on soil
582 properties and pedogenic processes along a lithosequence. Geoderma 249–250, 12-20.
583 Marschall, H., Meyer, C., Wunder, B., Ludwig, T. and Heinrich, W. (2009) Experimental boron isotope
584 fractionation between tourmaline and fluid: confirmation from in situ analyses by secondary ion
585 mass spectrometry and from Rayleigh fractionation modelling. Contr. Mineral. and Petrol. 158, 675-
586 681.

587 Martens, R., uuml and ller-Warmuth, W. (2000) Structural groups and their mixing in borosilicate
588 glasses of various compositions – an NMR study. Journal of Non-Crystalline Solids 265, 167-
589 175.
590 Millot, R., Gaillardet, J., Dupré, B. and Allègre, C.J. (2002) The global control of silicate weathering
591 rates and the coupling with physical erosion: new insights from rivers of the Canadian Shield. Earth
592 and Planetary Science Letters 196, 83-98.
593 Moore, D.C. and Singer, M.J. (1990) Crust Formation Effects on Soil Erosion Processes. 54, 1117-
594 1123.
595 Muttik, N., Kirsimäe, K., Newsom, H.E. and Williams, L.B. (2011) Boron isotope composition of
596 secondary smectite in suevites at the Ries crater, Germany: Boron fractionation in weathering and
597 hydrothermal processes. Earth and Planetary Science Letters 310, 244-251.
598 OECD (2000) Porewater Extraction from Argillaceous Rocks for Geochemical Characterisation.
599 Nuclear Energy Agency.
600 Powell, D.H., Tongkhao, K., Kennedy, S.J. and Slade, P.G. (1997) Interlayer water structure in Na- and
601 Li-montmorillonite clays. Physica B: Condensed Matter 241-243, 387-389.
602 Prigent, C., Guillot, S., Agard, P., Lemarchand, D., Soret, M. and Ulrich, M. (2018) Transfer of
603 subduction fluids into the deforming mantle wedge during nascent subduction: Evidence from trace
604 elements and boron isotopes (Semail ophiolite, Oman). Earth and Planetary Science Letters 484, 213-
605 228.
606 Rasmussen, C., Brantley, S., Richter, D.D., Blum, A., Dixon, J. and White, A.F. (2011) Strong climate
607 and tectonic control on plagioclase weathering in granitic terrain. Earth and Planetary Science Letters
608 301, 521-530.
609 Riebe, C.S., Hahm, W.J. and Brantley, S.L. (2017) Controls on deep critical zone architecture: a
610 historical review and four testable hypotheses. Earth Surface Processes and Landforms 42, 128-156.
611 Samuel, J., Rouault, R. and Besnus, Y. (1985) Analyse multiélémentaire standardisée des matériaux
612 géologiques en spectrométrie d'émission par plasma à couplage inductif = Geological materials
613 standardized multi-analysis with inductively-coupled plasma emission spectrometry. Analusis 13,
614 312-317.
615 Sanchez-Valle, C., Reynard, B., Daniel, I., Lecuyer, C., Martinez, I. and Chervin, J.-C. (2005) Boron
616 isotopic fractionation between minerals and fluids: New insights from in situ high pressure-high
617 temperature vibrational spectroscopic data. Geochimica et Cosmochimica Acta 69, 4301-4313.
618 Sikalidis, C.A., Alexiades, C. and Misaelides, P. (1989) Adsorption of uranium and thorium from
619 aqueous solutions by the clay minerals montmorillonite and vermiculite. Toxicological &
620 Environmental Chemistry 20-21, 175-180.
621 Skipper, N.T., Soper, A.K. and McConnell, J.D.C. (1991) The structure of interlayer water in
622 vermiculite. The Journal of Chemical Physics 94, 5751-5760.
623 Spivack, A.J., Palmer, M.R. and Edmond, J.M. (1987) The sedimentary cycle of the boron isotopes.
624 Geochimica et Cosmochimica Acta 51, 1939-1949.
625 Stevens, P.R. and Walker, T.W. (1970) The Chronosequence Concept and Soil Formation. The
626 Quarterly Review of Biology 45, 333-350.
627 Tonarini, S., Forte, C., Petrini, R. and Ferrara, G. (2003) Melt/biotite 11B/ 10B isotopic fractionation
628 and the boron local environment in the structure of volcanic glasses. Geochimica et Cosmochimica
629 Acta 67, 1863-1873.
630 Tournassat, C., Tinnacher, R.M., Grangeon, S. and Davis, J.A. (2018) Modeling uranium(VI) adsorption
631 onto montmorillonite under varying carbonate concentrations: A surface complexation model
632 accounting for the spillover effect on surface potential. Geochimica et Cosmochimica Acta 220, 291-
633 308.
634 Turner, B.F., White, A.F. and Brantley, S.L. (2010) Effects of temperature on silicate weathering:
635 Solute fluxes and chemical weathering in a temperate rain forest watershed, Jamieson Creek, British
636 Columbia. Chemical Geology 269, 62-78.
637 Turpault, M.P. (2006) Elements in soils: total and extractable contents, solid phase speciation.
638 Handbook of methods used in rhizosphere research, 237-239.

639 Turpault, M.P., Utérano, C., Boudot, J.P. and Ranger, J. (2005) Influence of mature Douglas fir roots
640 on the solid soil phase of the rhizosphere and its solution chemistry. Plant and Soil 275, 327-336.
641 Viers, J., Dupré, B. and Gaillardet, J. (2009) Chemical composition of suspended sediments in World
642 Rivers: New insights from a new database. Science of The Total Environment 407, 853-868.
643 Viville, D., Chabaux, F., Stille, P., Pierret, M.C. and Gangloff, S. (2012) Erosion and weathering fluxes in
644 granitic basins: The example of the Strengbach catchment (Vosges massif, eastern France). CATENA
645 92, 122-129.
646 Voinot, A., Lemarchand, D., Collignon, C., Granet, M., Chabaux, F. and Turpault, M.P. (2013)
647 Experimental dissolution vs. transformation of micas under acidic soil conditions: Clues from boron
648 isotopes. Geochimica et Cosmochimica Acta 117, 144-160.
649 White, A.F. (2008) Quantitative Approaches to Characterizing Natural Chemical Weathering Rates, in:
650 Brantley, S.L., Kubicki, J.D., White, A.F. (Eds.), Kinetics of Water-Rock Interaction. Springer New York,
651 New York, NY, pp. 469-543.
652 White, A.F., Bullen, T.D., Schulz, M.S., Blum, A.E., Huntington, T.G. and Peters, N.E. (2001) Differential
653 rates of feldspar weathering in granitic regoliths. Geochimica et Cosmochimica Acta 65, 847-869.
654 White, A.F., Schulz, M.S., Vivit, D.V., Blum, A.E., Stonestrom, D.A. and Harden, J.W. (2005) Chemical
655 weathering rates of a soil chronosequence on granitic alluvium: III. Hydrochemical evolution and
656 contemporary solute fluxes and rates. Geochimica et Cosmochimica Acta 69, 1975-1996.
657 Wild, B., Daval, D., Beaulieu, E., Pierret, M.-C., Viville, D. and Imfeld, G. (2019) In-situ dissolution rates
658 of silicate minerals and associated bacterial communities in the critical zone (Strengbach catchment,
659 France). Geochimica et Cosmochimica Acta 249, 95-120.
660 Williams, L.B. and Hervig, R.L. (2002) Exploring intra-crystalline B-isotope variations in mixed-layer
661 illite-smectite. American Mineralogist 87, 1564-1570.
662 Williams, L.B. and Hervig, R.L. (2005) Lithium and boron isotopes in illite-smectite: The importance of
663 crystal size. Geochimica et Cosmochimica Acta 69, 5705-5716.
664 Williams, L.B., Hervig, R.L., Holloway, J.R. and Hutcheon, I. (2001) Boron isotope geochemistry during
665 diagenesis. Part I. Experimental determination of fractionation during illitization of smectite.
666 Geochimica et Cosmochimica Acta 65, 1769-1782.
667 Xu, N., Braida, W., Christodoulatos, C. and Chen, J. (2013) A Review of Molybdenum Adsorption in
668 Soils/Bed Sediments: Speciation, Mechanism, and Model Applications. Soil and Sediment
669 Contamination: An International Journal 22, 912-929.
670 Yamaoka, K., Hong, E., Ishikawa, T., Gamo, T. and Kawahata, H. (2015) Boron isotope geochemistry of
671 vent fluids from arc/back-arc seafloor hydrothermal systems in the western Pacific. Chemical
672 Geology 392, 9-18.
673 Yamaoka, K., Ishikawa, T., Matsubaya, O., Ishiyama, D., Nagaishi, K., Hiroyasu, Y., Chiba, H. and
674 Kawahata, H. (2012) Boron and oxygen isotope systematics for a complete section of oceanic crustal
675 rocks in the Oman ophiolite. Geochimica et Cosmochimica Acta 84, 543-559.
676 Zeng, Z., Wang, X., Chen, C.-T.A., Yin, X., Chen, S., Ma, Y. and Xiao, Y. (2013) Boron isotope
677 compositions of fluids and plumes from the Kueishantao hydrothermal field off northeastern Taiwan:
678 Implications for fluid origin and hydrothermal processes. Marine Chemistry 157, 59-66.

679

Effect of a strong desire to void on walking speed in individuals with multiple sclerosis and urinary disorders

Abstract

Background. Lower urinary tract symptoms, especially overactive bladder, are frequent and disabling in individuals with multiple sclerosis (IwMS). An association with gait disorders is common, which could aggravate continence difficulties and affect quality of life. The association between the need to void and walking has never been studied in this population.
Objective. The primary aim of this study was to assess the effect of a strong desire to void (SDV) on walking speed in IwMS and lower urinary tract symptoms. The secondary aim was to identify clinical or urodynamic factors associated with walking speed impairment at SDV in this population.

Methods. We included IwMS with urinary disorders and Expanded Disability Status Scale score < 7 in this observational study. Individuals underwent 3 10-m walk tests (10MWT) and one Timed Up and Go (TUG) test at SDV and at post-void (PV).

Results. Among the 72 IwMS included (mean [SD] age 50.6 [11.6] years; 46 [64%] females), the mean (SD) speed for 10MWT was 1.00 (0.31) $m.s^{-1}$ at SDV and 1.07 (0.30) $m.s^{-1}$ at PV ($p<0.0001$). Time for TUG was also increased when individuals felt SDV: mean 11.53 (4.6) sec at SDV versus 10.77 (3.8) sec at PV ($p=0.004$). No predictors of greater impairment of walking speed at SDV were identified.

Conclusion. This study suggests a clinical impact of bladder sensation on walking speed in IwMS and urinary disorders. None of the individual characteristics could predict greater decrease in gait velocity at SDV.

Keywords: Multiple sclerosis, Walking speed, Gait, Urination, Lower urinary tract symptoms

Introduction

Multiple sclerosis (MS) causes demyelinating lesions and could be responsible for a number of symptoms, including motor or sensitivity disorders, cognitive impairment, visual disturbances, and urinary and bowel disorders. Gait difficulties are the most visible disability, and about 70% of patients report a psychological impact due to their walking impairment[1]. Different neurological presentations can be observed in different individuals: spastic, ataxic, cerebellar, and pyramidal forms, depending on the topography of the cerebral or medullar lesions. Lower urinary tract symptoms (LUTSs) are also very common, with a prevalence of 32% to 86%[2]. Overactive bladder with urgency, increased bladder frequency and urgency urinary incontinence is the most common symptoms. Obstructive symptoms are also frequent and may coexist with storage symptoms. Detrusor overactivity is the most frequent urodynamic profile, but the correlation between clinical symptoms and urodynamics data is not perfect. Other urodynamic profiles exist: bladder oversensitivity, detrusor-sphincter dyssynergia, and neurogenic detrusor underactivity, but urodynamics can be normal for 1% to 34% of patients with LUTSs[2,3]. Despite a correlation between frequency and severity of LUTSs and severity of incapacity assessed by Expanded Disability Status Scale (EDSS) [4] or with number of falls[5], no strict relationship can be demonstrated between type of LUTS, urodynamics profile and type of neurological presentation (pyramidal, with or without major spasticity, cerebellar etc.)[4,6].

The role of bladder filling and need to void on gait has been poorly studied and only in healthy populations. Yet, some hypotheses could support a link between these 2 parameters.

The need to void is a sensory stimulus, integrated in different cerebral areas, including insula, periaqueductal gray, cingulate cortex, hypothalamus and prefrontal area[7,8]. A modification in gait velocity with emotions was demonstrated. Jousse et al. showed a decrease in attentional skills with a strong desire to void (SDV)[9]. These 2 studies may suggest a possible impact of the need to void on gait velocity, as a new sensory phenomenon to integrate and modulate, as a function of the locomotion task.

At the medullar stage, a modification of the H-reflex was demonstrated at SDV in healthy individuals[10]. The H-reflex is considered to reflect motoneuronal excitability. The impact of motoneuronal excitability on gait is not clearly established, but some studies revealed a modification of the H-reflex with gait velocity[11,12]. The H-reflex is also used as an indirect measure of spasticity, but its expression is not correlated with spasticity severity[13]. The modulation of the medullar reflex with bladder sensation, and perhaps with bladder filling or detrusor overactivity, with a possible impact on gait may explain a link between gait and the need to void.

The consequences of the need to void on other tasks have been little studied and only in healthy populations; however, alterations in attentional condition[9], gait velocity[14] and balance[15] performance were shown. Assessing the effect of the need to void in a neurologic population with frequent gait disorders and LUTSs could be pertinent to better understand the pathophysiological mechanisms and evaluate whether an intervention for one condition may improve the other, with the hypothesis that an appropriate management of LUTSs could lead to an improvement in some locomotor parameters.

The primary aim of this study was to assess the effect of an SDV on gait in individuals with multiple sclerosis (IwMS) and LUTSs. The secondary aim was to identify clinical or

urodynamic factors (EDSS, symptom severity, detrusor overactivity, cystometric capacity) associated with greater gait impairment.

Material and methods

Participants

Individuals over age 18 who were consulting for LUTSs linked with MS in the neuro-urology department of a university hospital between February 2017 and March 2017 were invited to participate in this observational study. Individuals who agreed to participate were included where they were admitted for a consultation or urodynamic assessment, and all tests were performed on the same day.

Inclusion criteria were MS with EDSS score 1 to 6.5 and LUTSs secondary to MS (storage or voiding symptoms). Participants had to be able to walk 50 m without human help and to hold urine for 5 min, the time required to perform the tests. They could be taking medication for MS or LUTSs. All types of MS were accepted. We excluded individuals with urinary tract infections, relapse of MS in the last 7 days, or severe cognitive impairment (Mini Mental State Examination [MMSE] score < 10).

Measures and procedure

Gait was assessed by 2 clinical tests approved for MS. The same tests were performed under 2 conditions: first when the individual felt an SDV, and then immediately after micturition, spontaneously or with self-catheterization (post-void [PV]).

The primary outcome was gait velocity assessed by a 10-m walk test (10MWT)[16]. Three trials were recorded, as per Booth et al. [14]. Individuals were instructed to walk the 10 m at a comfortable speed. Maximum speed was not recorded to limit the impact of fatigue on test repetition, because maximal speed improves energetic cost. Only the 6 intermediate meters (meters 2 to 8) were recorded, to limit the effect of acceleration and deceleration. Tests were recorded with a manual chronometer by the same examiner for each individual, with 30 sec of rest at most between each trial.

Secondary outcomes were time on the Timed Up and Go Test (TUG)[17,18] and gait variability assessed by the coefficient of variation (CoV) of the 3 trials of 10MWT. The trial began with a non-recorded TUG to understand instructions and to limit the learning effect, but only one trial was recorded to limit the test duration and fatigue induced by the get up exertion.

Medical history, treatment, and anthropometric data were collected. An MMSE was administered to identify memory impairment. Urinary symptoms were assessed by the questionnaire Urinary Symptom Profile (USP) with 3 aspects: “stress urinary incontinence” (/9), “overactive bladder” (/21) and “low stream” (/9)[19]. Data for the last cystometry were collected (retrospectively if cystometry was not planned on the day of inclusion): detrusor overactivity, volume at first detrusor contraction, SDV during filling, and cystometric capacity. MS severity was assessed by the EDSS, a score based on measures of impairment in 8 functional systems, and on walking ability[20]. Individuals with an EDSS score > 4 complained of gait difficulties. Each participant was asked if they had urine leakage during the tests. PV residual volume was measured with a mobile transabdominal ultrasound apparatus (Bladder Scan®); 3 measures were taken, and the highest was recorded. Secondary analyses were planned to identify clinical or urodynamic factors associated with greater gait impairment: age, EDSS score, need for a walking device, severity of overactive bladder on

USP score, spontaneous void or self-catheterization, cognitive impairment assessed by the MMSE, detrusor overactivity during the last cystometry, and PV residual volume.

Ethics approval

The study protocol and data collection were conducted in accordance with the ethical standards of the national research committee and the Declaration of Helsinki. This study was approved by the local ethics committee (registration no. 2015-A00125-44). All participants gave their consent to participate. This study was registered on ClinicalTrials.gov: NCT03204747.

Statistical analysis

Statistical tests were performed with R for Windows (Rx64 3.2.3). In a previous study of healthy individuals, the only one assessing the effect of the need to void on gait, Booth et al. [14] showed a mean difference on gait velocity of 0.05 $m.s^{-1}$ between SDV and PV. In IwMS, we expected a slightly greater mean difference between the 2 conditions. Thus, based on this previous study, for an expected mean difference of 0.06 $m.s^{-1}$, a standard deviation of 0.17 (SD 0.18 to 0.19 in the Booth et al. study) and 80% power, we needed 65 participants. Mean gait velocity at SDV and PV were calculated for the 3 trials of 10MWT. Variability of the 3 trials was assessed by the CoV (standard deviation/average). The temporal parameters of gait for 10MWT, TUG and CoV data were normally distributed. Thus, these were analyzed by Student's *t* test for paired samples. The effect size was calculated with Cohen's d formula. The impact of clinical and urodynamic parameters on the mean difference between TM10 at SDV and PV were analyzed by Student *t* test for qualitative variables and Spearman

correlation for quantitative variables. Significance was considered at $p < 0.05$. Missing data were not replaced.

Results

We included 72 individuals (mean [SD] age 50.6 [11.6] years; 46 [64%] females). Characteristics are summarized in Table 1. Three individuals performed only 2 trials of the 10MWT for each condition because of physical tiredness. The mean speed for 10MWT was 1.00 (0.31) $m.s^{-1}$ at SDV and 1.07 (0.30) $m.s^{-1}$ at PV ($p<0.0001$; effect size 0.79). Maximal improvement on mean 10MWT was 0.34 $m.s^{-1}$ (5.03 s). Only 10 (14%) participants had a lower performance at PV than SDV. These 10 participants and the others did not differ in EDSS score, use of a walking device, existence of detrusor overactivity, or age. The distribution of gait velocity change between SDV and PV is presented in the Figure. The individual variability of the 3 trials of 10MWT, assessed by the CoV, was significant (mean [SD] 5.2% [3.9] vs 4.2% [3.6], $p=0.048$). Between the first and second try, 47% of participants showed improved gait velocity at SDV and 40% at PV. Between the second and third try, 68% of participants showed improved gait velocity at SDV and 63% at PV. Mean time for TUG was also increased when individuals felt SDV: 11.53 (4.6) sec at SDV versus 10.77 (3.8) sec at PV ($p=0.004$, effect size 0.35). Only one participant reported a leak during the test.

Secondary analysis did not identify any predictors of greater impairment of walking speed at SDV among the features explored (Tables 2 and 3).

Discussion

The results of this study showed an increase in gait velocity after voiding as compared with velocity during an SDV in lwMS and urinary disorders. This finding suggests a negative impact of an urgent need to void on walking speed in IwMS and urinary disorders. No clinical or urodynamic factors were found to predict greater reduction in gait performance.

In their study, Booth et al.[14] proposed that “the experience represents a dual task or divided attention situation” to explain the difference in the SDV and PV situation in healthy individuals. The authors introduced for the first time bladder sensation as a divided attention situation. The role of dual tasks is well established, particularly in older adults and with a risk of falling. The effect of dual tasks, in particular in gait, has been widely studied and demonstrated in IwMS. In a recent review, the presence of cognitive motor interference appeared more frequent in IwMS than in healthy individuals during gait analysis [21]. Individuals with mild cognitive impairment seemed more sensitive to the influence of a cognitive task on walking speed[22]. Moreover, emotional perception of the need to void could also influence gait velocity.

Functional MRI shows activation of different areas during bladder filling (insula, periaqueductal gray, cingulate cortex, hypothalamus and prefrontal area, amygdala). Most of these cerebral areas are implicated in emotional control, and functional MRI studies found less activation or deactivation of some of these areas in individuals with overactive bladder as compared with healthy individuals, which suggests a lack of control of this unpleasant sensation[23]. A modification of gait velocity has been found correlated with emotion in healthy individuals[24]. In IwMS, only the fear of falling has been studied, but other emotions could also affect gait. We found no relationship between severity of symptoms and greater difference between the 2 conditions. However, the proportion of individuals with regular

leaks was higher (no statistical analysis) in individuals with a difference of > 0.1 m/s between SDV and PV, which supports a possible distractible effect of the urge to void and the role of emotional control.

A second explanation is the effect of bladder sensation on motoneuronal excitability. Previous studies of individuals with spinal cord injury evoked a gait spinal central pattern generator[25,26]. Furthermore, the H-reflex, which is a spinal motoneuronal response to electrical stimulation, is considered to reflect motoneuronal excitability. Variation in H-reflex amplitude reflects modified spinal cell excitability [27]. During gait, some studies showed an increase in H-reflex amplitude, which suggests an increase in motoneuronal excitability, with variation in function of gait cycle. A proportional increase in the amplitude of the H-reflex as a function of walking speed has been demonstrated[11,12]. Thus, a role of motoneuronal excitability in gait velocity can be supposed, and a decrease in motoneuronal excitability could affect walking speed. A decrease in H-reflex in the soleus muscle occurs at SDV in healthy individuals[10]. However, no study has examined the impact of the need to void on motoneuronal excitability in IwMS, whereas in individuals with spinal cord injury, bladder filling tends to increase H-reflex amplitude[10]. Application of these findings in IwMS is difficult, as far as lesion localizations at cerebral or medullar level could affect H-reflex variability, and a specific study would be necessary.

Another possible explanation is that pelvic and trunk muscle activation is modified by bladder filling: the activation of pelvic floor muscles decreases when the bladder is moderately full, and the obliquus internus abdominis and rectus abdominis activation is increased. Bladder fullness also influences balance: an increase in center-of-pressure motions on a force plate was demonstrated when the bladder was full in healthy individuals[15]. These 2 parameters could participate in gait velocity decrease at SDV.

Our results agree with the Booth et al.[14] study of healthy individuals (continent, International Prostate Symptom Score 0-7). The authors used a GAITRite® walkway and showed an impairment of 0.05 $m.s^{-1}$ at SDV as compared with PV. Results in our study were obtained with clinical (not instrumental) tests. A potential limitation of the primary outcome is that fast speed usually has better reliability in 10MWT than comfortable speed, but energetic cost is improved at maximal speed. We chose not to record this measure to limit the impact of fatigue on the different tests.

Several measures were established to limit bias in recording walking tests. Participants underwent 3 trials for the 10MWT under each condition, to limit intra-individual variability and to observe whether this variability is modified by SDV, as previously described[14]. To prevent inter-judge variation, all tests were recorded by the same examiner using a standardized protocol and the same time-measuring tool. A recent study did not find a significant difference between 3 consecutive short walk tests (Timed 25-Foot Walk) [28], which suggests no spontaneous improved performance with repeated tests. Thus, to reduce the impact of tiredness on recording, we did not randomize by order of condition, and clinical tests at PV were always performed after those at SDV. This minimization of bias is also a potential limitation for highlighting a greater difference between the 2 conditions, because fatigue induced by the first tests can affect subsequent performance with a limited rest time between the 2 conditions. Individuals could also take a rest between the tests to reduce this bias. Our results did not reveal a progressive improvement in performance with the repetition of tests during the same condition. This suggests that the difference shown between SDV and PV is not related to a spontaneous improvement due to the repetition of the same exercise. For the TUG test, the learning effect was limited by a first non-recorded trial to verify comprehension of instructions. Instructions were repeated before each trial to facilitate their memorization.

Our study has several limitations. Clinical tests are less precise than instrumental tests, and some gait parameters such as stride length, swing time, and duration of single support could not be studied. The examiner was not blinded to condition (PV or SDV), but participants did not know the expected results and were not informed of the time performed in each test. The sequence of the test after urination can have a negative impact on performance, by the fatigue induced by the first tests and by the fatigue induced by urination, with the different stages of undressing, sitting, etc. This could influence the identification of factors associated with a greater impact of the need to void on walking speed. Moreover, because of the design of the study, the negative impact of the urgent need to void is derived from the interpretation of the increase in speed after urination. An evaluation without the need to void but away from urination could have been interesting to free oneself from possible neurological reflexes induced by micturition, especially in individuals with detrusor overactivity. In secondary analyses, an evaluation of executive functions would have allowed a more specific analysis, in the hypothesis of “dual task” impact, because the MMSE does not properly evaluate these functions.

The difference between SDV and PV we found is less than the minimally clinical relevant differences described in the literature, but these have been defined with small numbers of participants with high EDSS score or using a modification of EDSS score as a relevant clinical change, but the EDSS score is not sensitive to minor change[29–31]. Thus, the observed difference in our study can be difficult to interpret; we did not expect a clinical state change as a modification of the EDSS score between SDV and PV, and the comparison of our results with the mentioned thresholds is not wholly adapted (median EDSS or condition to realize the 10MWT differed from those of our study). Therefore, clinical interpretation of this PV improvement is subtle, and our data cannot lead to specific clinical recommendations.

There are many different perspectives from this study. First, a new study of the specific population within IwMS could improve the accuracy of results and clinical relevance. The role of detrusor overactivity was not shown, but there was likely a lack of power in secondary analysis, and owing to the study design, 27 of the 62 urodynamic data measurements available were older than 3 months. Also, all individuals did not have urodynamics data, and some measurements were prior to the inclusion date, which limits their interpretation. Further research is necessary to judge the influence on spasticity. Several conditions modify spasticity: urinary tract infections, ingrown nails, lithiasis, temperature[32]. Yet, the possibility of spasticity exacerbation during detrusor uninhibited contraction has never been considered. Moreover, considering the impact of the need to void as a dual task requires a comparison with cognitive tasks during gait evaluation, especially since an impact on attention skills has been demonstrated[9].

Finally, our study suggests that clinical walk tests are sensitive to changes in individual variations such as the need to void. The use of the tests in clinical practice and research must be standardized, to reduce bias in their interpretation and clinical significance.

Conclusion

This study suggests decreased walking speed at SDV in IwMS and urinary disorders, showing an increase in gait velocity after voiding with an SDV. Severity of disability and urodynamic parameters were not associated with greater difference in velocity at SDV than PV, but the heterogeneity of the MS population could suggest lack of power in our study to demonstrate the influence of a specific factor.

Funding. Dr. Hentzen reports grants from SIFUD-PP (the francophone society of urodynamics) and from LILIAL-GREEN GRC-01 UPMC (Group of clinical REsEarch in Neurourology), during the conduct of the study.

Conflict of interest. No conflict of interest in relation to the study.

Legend

Figure. Walking speed change between post-void and a strong desire to void.

References

[1] Larocca NG. Impact of walking impairment in multiple sclerosis: perspectives of patients and care partners. The Patient 2011;4:189–201. doi:10.2165/11591150-000000000-00000.

[2] de Sèze M, Ruffion A, Denys P, Joseph P-A, Perrouin-Verbe B, GENULF. The neurogenic bladder in multiple sclerosis: review of the literature and proposal of management guidelines. Mult Scler Houndmills Basingstoke Engl 2007;13:915–28. doi:10.1177/1352458506075651.

[3] Fragalà E, Russo GI, Di Rosa A, Giardina R, Privitera S, Favilla V, et al. Association Between the Neurogenic Bladder Symptom Score and Urodynamic Examination in Multiple Sclerosis Patients With Lower Urinary Tract Dysfunction. Int Neurourol J 2015;19:272–7. doi:10.5213/inj.2015.19.4.272.

[4] Koldewijn EL, Hommes OR, Lemmens WA, Debruyne FM, van Kerrebroeck PE. Relationship between lower urinary tract abnormalities and disease-related parameters in multiple sclerosis. J Urol 1995;154:169–73.

[5] Sung J, Shen S, Motl RW, Sosnoff JJ. Bladder function and falls in individuals with multiple sclerosis. Disabil Rehabil 2016;38:2193–7. doi:10.3109/09638288.2015.1123311.

[6] Giannantoni A, Scivoletto G, Di Stasi SM, Grasso MG, Finazzi Agrò E, Collura G, et al. Lower urinary tract dysfunction and disability status in patients with multiple sclerosis. Arch Phys Med Rehabil 1999;80:437–41.

[7] Athwal BS, Berkley KJ, Hussain I, Brennan A, Craggs M, Sakakibara R, et al. Brain responses to changes in bladder volume and urge to void in healthy men. Brain J Neurol 2001;124:369–77. doi:10.1093/brain/124.2.369.

[8] Khavari R, Karmonik C, Shy M, Fletcher S, Boone T. Functional Magnetic Resonance

311 Imaging with Concurrent Urodynamic Testing Identifies Brain Structures Involved in Micturition
312 Cycle in Patients with Multiple Sclerosis. J Urol 2017;197:438–44. doi:10.1016/j.juro.2016.09.077.

313 [9] Jousse M, Verollet D, Guinet-Lacoste A, Le Breton F, Auclair L, Sheikh Ismael S, et al. Need
314 to void and attentional process interrelationships. BJU Int 2013;112:E351-357. doi:10.1111/bju.12224.

315 [10] Inghilleri M, Carbone A, Pedace F, Conte A, Frasca V, Berardelli A, et al. Bladder filling
316 inhibits somatic spinal motoneurones. Clin Neurophysiol Off J Int Fed Clin Neurophysiol
317 2001;112:2255–60.

318 [11] Simonsen EB, Dyhre-Poulsen P. Amplitude of the human soleus H reflex during walking and
319 running. J Physiol 1999;515 (Pt 3):929–39. doi:10.1111/j.1469-7793.1999.929ab.x.

320 [12] Hodapp M, Klisch C, Berger W, Mall V, Faist M. Modulation of soleus H-reflexes during gait
321 in healthy children. Exp Brain Res 2007;178:252–60. doi:10.1007/s00221-006-0730-1.

322 [13] Voerman GE, Gregoric M, Hermens HJ. Neurophysiological methods for the assessment of
323 spasticity: the Hoffmann reflex, the tendon reflex, and the stretch reflex. Disabil Rehabil 2005;27:33–
324 68.

325 [14] Booth J, Paul L, Rafferty D, Macinnes C. The relationship between urinary bladder control
326 and gait in women. Neurourol Urodyn 2013;32:43–7. doi:10.1002/nau.22272.

327 [15] Smith MD, Coppieters MW, Hodges PW. Is balance different in women with and without
328 stress urinary incontinence? Neurourol Urodyn 2008;27:71–8. doi:10.1002/nau.20476.

329 [16] Paltamaa J, West H, Sarasoja T, Wikström J, Mälkiä E. Reliability of physical functioning
330 measures in ambulatory subjects with MS. Physiother Res Int J Res Clin Phys Ther 2005;10:93–109.

331 [17] Sebastião E, Sandroff BM, Learmonth YC, Motl RW. Validity of the Timed Up and Go Test
332 as a Measure of Functional Mobility in Persons With Multiple Sclerosis. Arch Phys Med Rehabil
333 2016;97:1072–7. doi:10.1016/j.apmr.2015.12.031.

334 [18] Valet M, Lejeune T, Devis M, van Pesch V, El Sankari S, Stoquart G. Timed up-and-go and 2-
335 minute walk test in patients with multiple sclerosis with mild disability: reliability, responsiveness and
336 link with perceived fatigue. Eur J Phys Rehabil Med 2018. doi:10.23736/S1973-9087.18.05366-2.

337 [19] Haab F, Richard F, Amarenco G, Coloby P, Arnould B, Benmedjahed K, et al. Comprehensive
338 evaluation of bladder and urethral dysfunction symptoms: development and psychometric validation
339 of the Urinary Symptom Profile (USP) questionnaire. Urology 2008;71:646–56.
340 doi:10.1016/j.urology.2007.11.100.

341 [20] Kurtzke JF. Rating neurologic impairment in multiple sclerosis: an expanded disability status
342 scale (EDSS). Neurology 1983;33:1444–52.

343 [21] Postigo-Alonso B, Galvao-Carmona A, Benítez I, Conde-Gavilán C, Jover A, Molina S, et al.
344 Cognitive-motor interference during gait in patients with Multiple Sclerosis: a mixed methods
345 Systematic Review. Neurosci Biobehav Rev 2018;94:126–48. doi:10.1016/j.neubiorev.2018.08.016.

346 [22] Lee J, Park S. Effects of a priority-based dual task on gait velocity and variability in older
347 adults with mild cognitive impairment. J Exerc Rehabil 2018;14:993–7.
348 doi:10.12965/jer.1836402.201.

[23] Griffiths D, Tadic SD. Bladder control, urgency, and urge incontinence: Evidence from functional brain imaging. Neurourol Urodyn 2008;27:466–74. doi:10.1002/nau.20549.

[24] Kang GE, Gross MM. The effect of emotion on movement smoothness during gait in healthy young adults. J Biomech 2016;49:4022–7. doi:10.1016/j.jbiomech.2016.10.044.

[25] Calancie B, Needham-Shropshire B, Jacobs P, Willer K, Zych G, Green BA. Involuntary stepping after chronic spinal cord injury. Evidence for a central rhythm generator for locomotion in man. Brain J Neurol 1994;117 (Pt 5):1143–59. doi:10.1093/brain/117.5.1143.

[26] Bussel B, Roby-Brami A, Néris OR, Yakovleff A. Evidence for a spinal stepping generator in man. Paraplegia 1996;34:91–2.

[27] Petersen N, Christensen LO, Nielsen J. The effect of transcranial magnetic stimulation on the soleus H reflex during human walking. J Physiol 1998;513 (Pt 2):599–610. doi:10.1111/j.1469-7793.1998.599bb.x.

[28] Meyer C, Killeen T, Lörincz L, Curt A, Bolliger M, Linnebank M, et al. Repeated assessment of key clinical walking measures can induce confounding practice effects. Mult Scler Houndmills Basingstoke Engl 2019:1352458519845839. doi:10.1177/1352458519845839.

[29] de Groot V, Beckerman H, Uitdehaag BMJ, de Vet HCW, Lankhorst GJ, Polman CH, et al. The usefulness of evaluative outcome measures in patients with multiple sclerosis. Brain J Neurol 2006;129:2648–59. doi:10.1093/brain/awl223.

[30] Vaney C, Blaurock H, Gattlen B, Meisels C. Assessing mobility in multiple sclerosis using the Rivermead Mobility Index and gait speed. Clin Rehabil 1996;10:216–26. doi:10.1177/026921559601000306.

[31] Learmonth YC, Paul L, McFadyen AK, Mattison P, Miller L. Reliability and clinical significance of mobility and balance assessments in multiple sclerosis. Int J Rehabil Res Int Z Rehabil Rev Int Rech Readaptation 2012;35:69–74. doi:10.1097/MRR.0b013e328350b65f.

[32] Chiara T, Carlos J, Martin D, Miller R, Nadeau S. Cold effect on oxygen uptake, perceived exertion, and spasticity in patients with multiple sclerosis. Arch Phys Med Rehabil 1998;79:523–8.

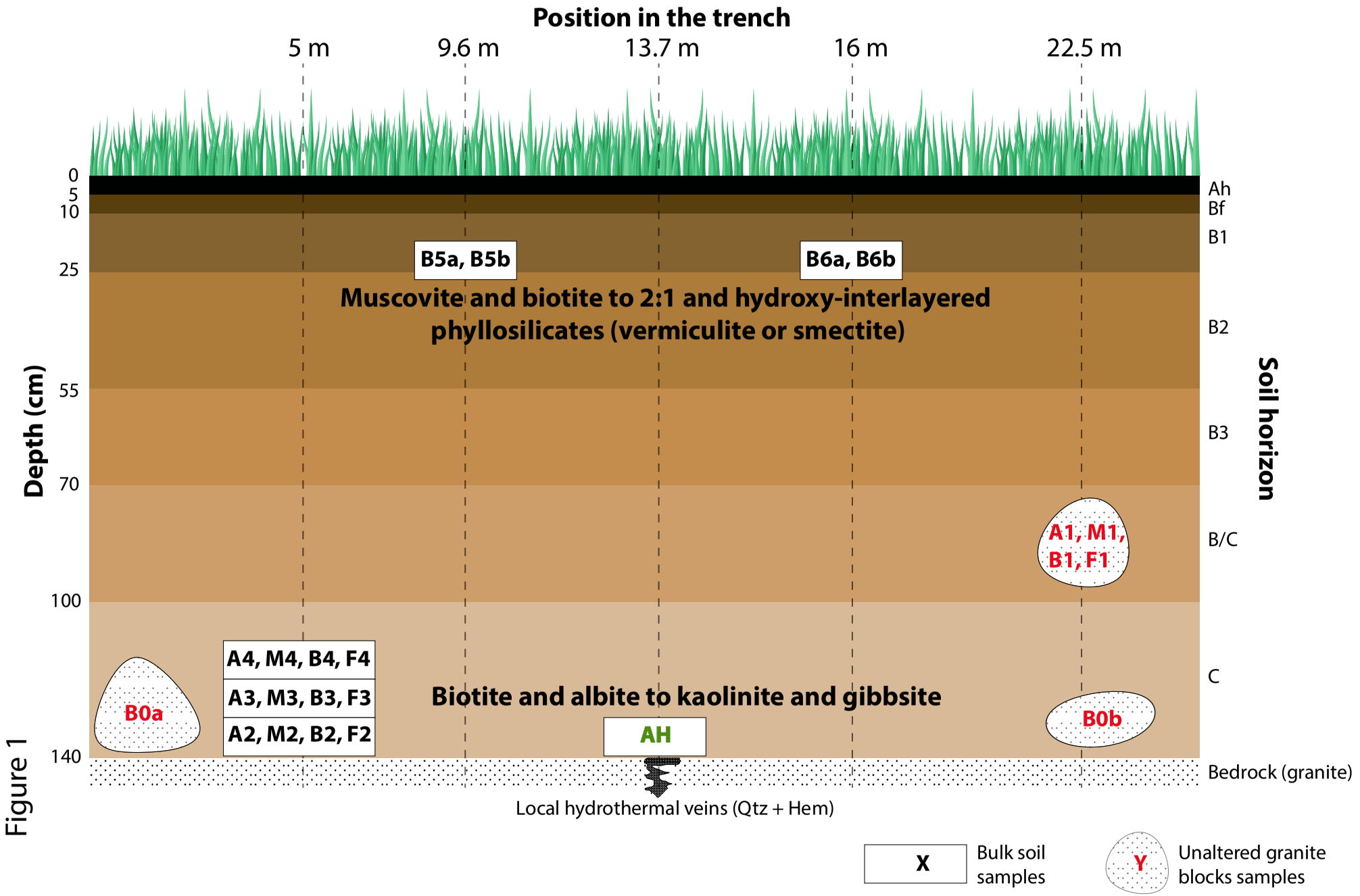
Position in the trench
5 m
9.6 m
13.7 m
16 m
22.5 m
Depth (cm)
0
5
10
25
55
70
100
140
Ah
Bf
B1
B2
B3
B/C
C
Soil horizon
B5a, B5b
B6a, B6b
Muscovite and biotite to 2:1 and hydroxy-interlayered phyllosilicates (vermiculite or smectite)
A1, M1, B1, F1
A4, M4, B4, F4
A3, M3, B3, F3
A2, M2, B2, F2
Biotite and albite to kaolinite and gibbsite
B0a
B0b
AH
Bedrock (granite)
Local hydrothermal veins (Qtz + Hem)
X
Bulk soil samples
Y
Unaltered granite blocks samples

Figure 1

Figure 2

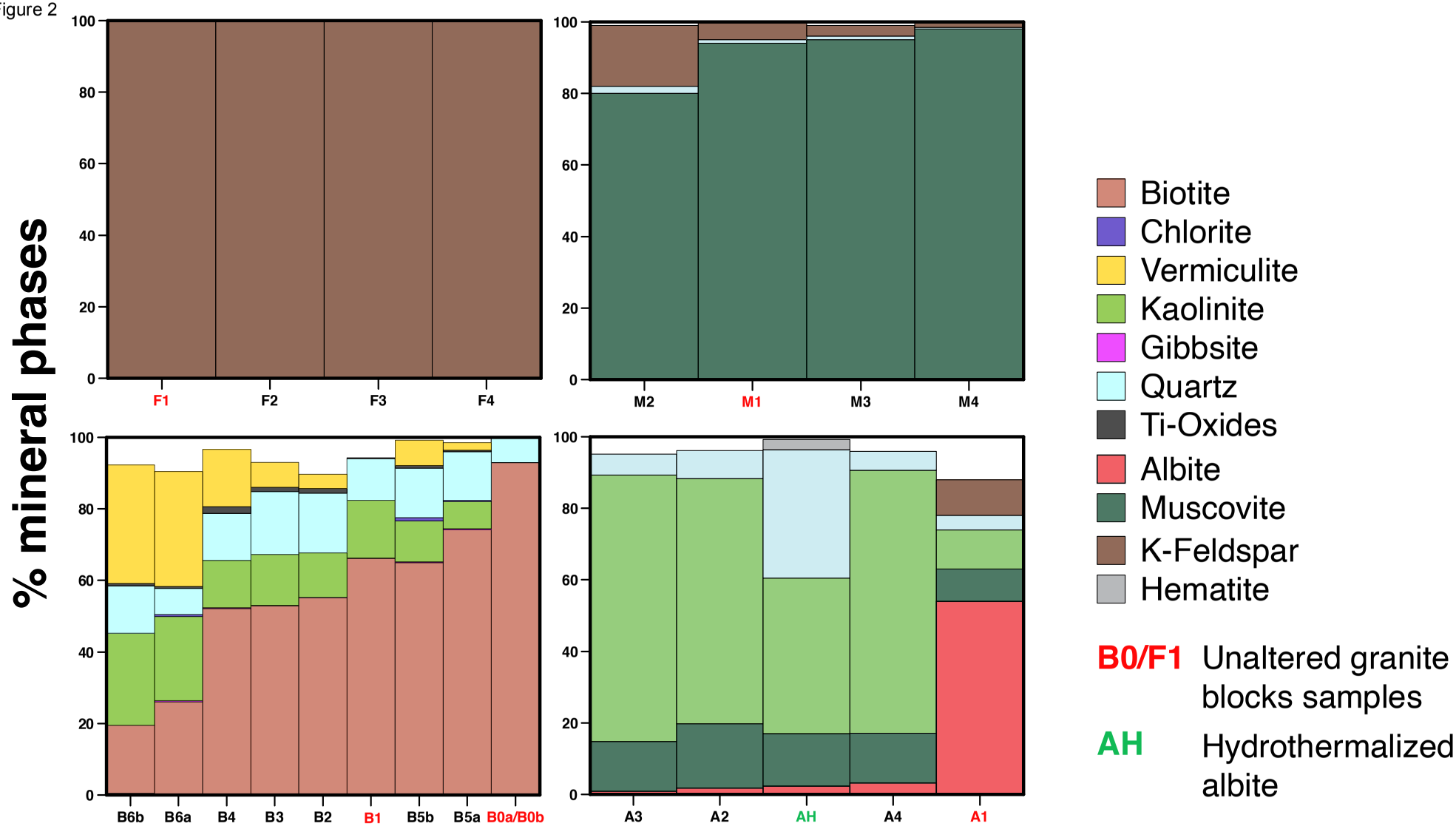
% mineral phases
100
80
60
40
20
0
F1
F2
F3
F4
M2
M1
M3
M4
B6b
B6a
B4
B3
B2
B1
B5b
B5a
B0a/B0b
A3
A2
AH
A4
A1
Biotite
Chlorite
Vermiculite
Kaolinite
Gibbsite
Quartz
Ti-Oxides
Albite
Muscovite
K-Feldspar
Hematite
B0/F1 Unaltered granite blocks samples
AH Hydrothermalized albite

figure 3

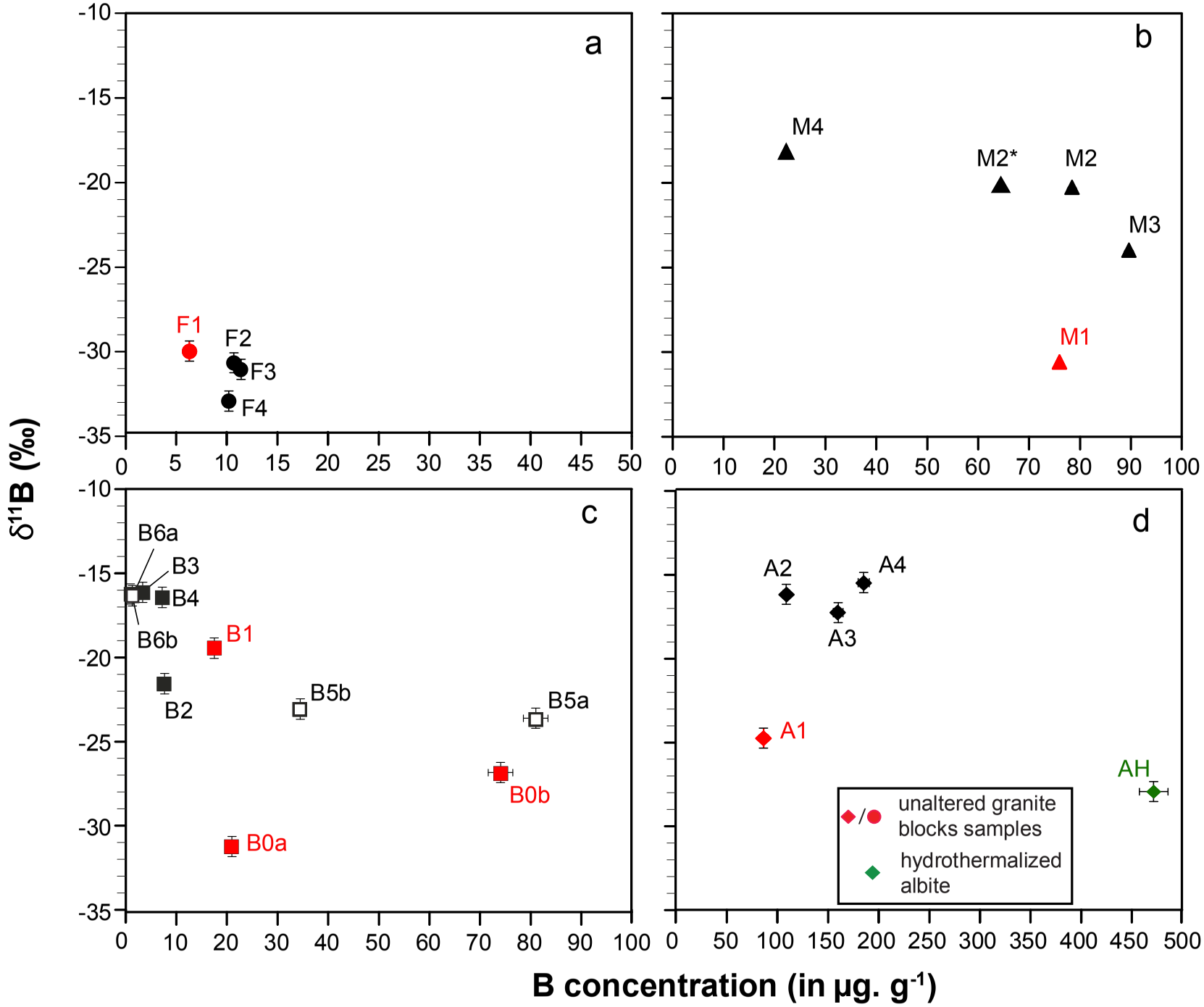
a
b
c
d
F1
F2
F3
F4
M4
M2*
M2
M3
M1
B6a
B3
B4
B6b
B1
B2
B5b
B5a
B0b
B0a
A2
A4
A3
A1
AH
unaltered granite blocks samples
hydrothermalized albite
δ11B (‰)
B concentration (in µg. g-1)

Figure 4

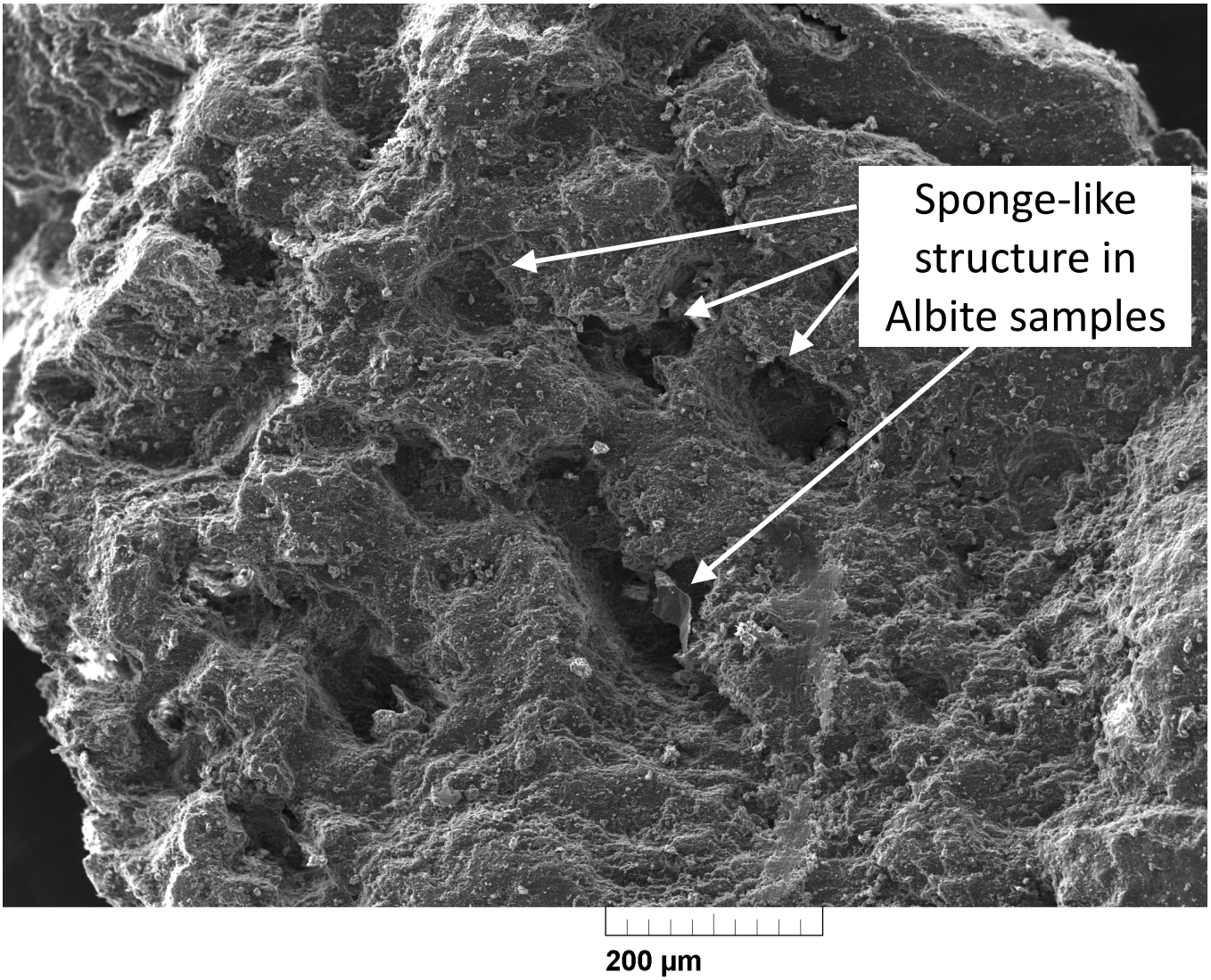

figure 5

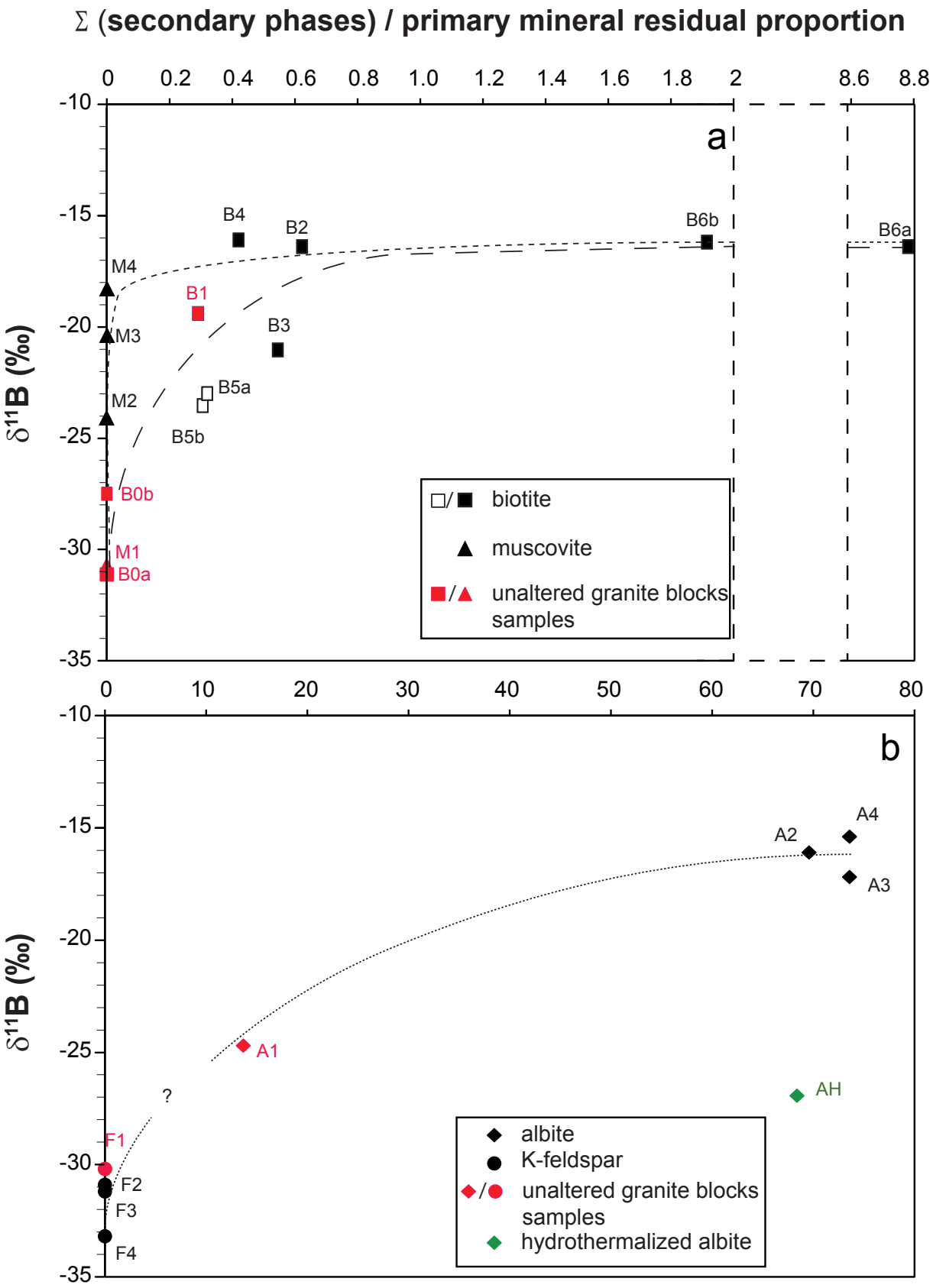
Σ (secondary phases) / primary mineral residual proportion
δ11B (‰)
a
b
biotite
muscovite
unaltered granite blocks samples
albite
K-feldspar
hydrothermalized albite
B4
B2
B6b
B6a
B1
B3
B5a
B5b
M4
M3
M2
M1
B0b
B0a
A4
A2
A3
A1
AH
F1
F2
F3
F4
?

figure 6

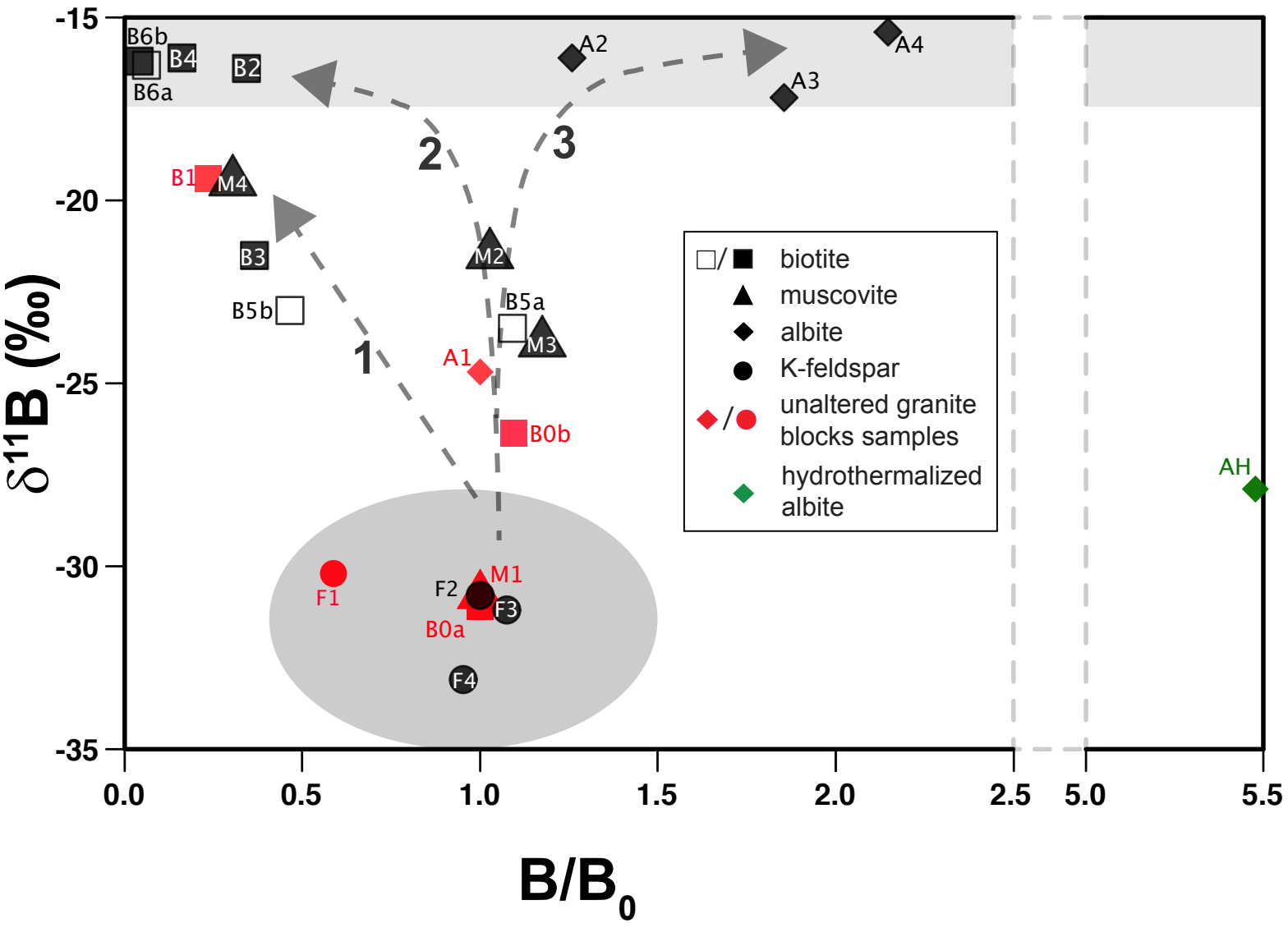
-15
-20
-25
-30
-35
$\delta^{11}B$ (‰)
0.0
0.5
1.0
1.5
2.0
2.5
5.0
5.5
B/B_0
B6b
B4
B6a
B2
A2
A4
A3
B1
M4
B3
B5b
M2
B5a
M3
A1
B0b
AH
F1
M1
F2
F3
B0a
F4
1
2
3
biotite
muscovite
albite
K-feldspar
unaltered granite blocks samples
hydrothermalized albite

figure A1

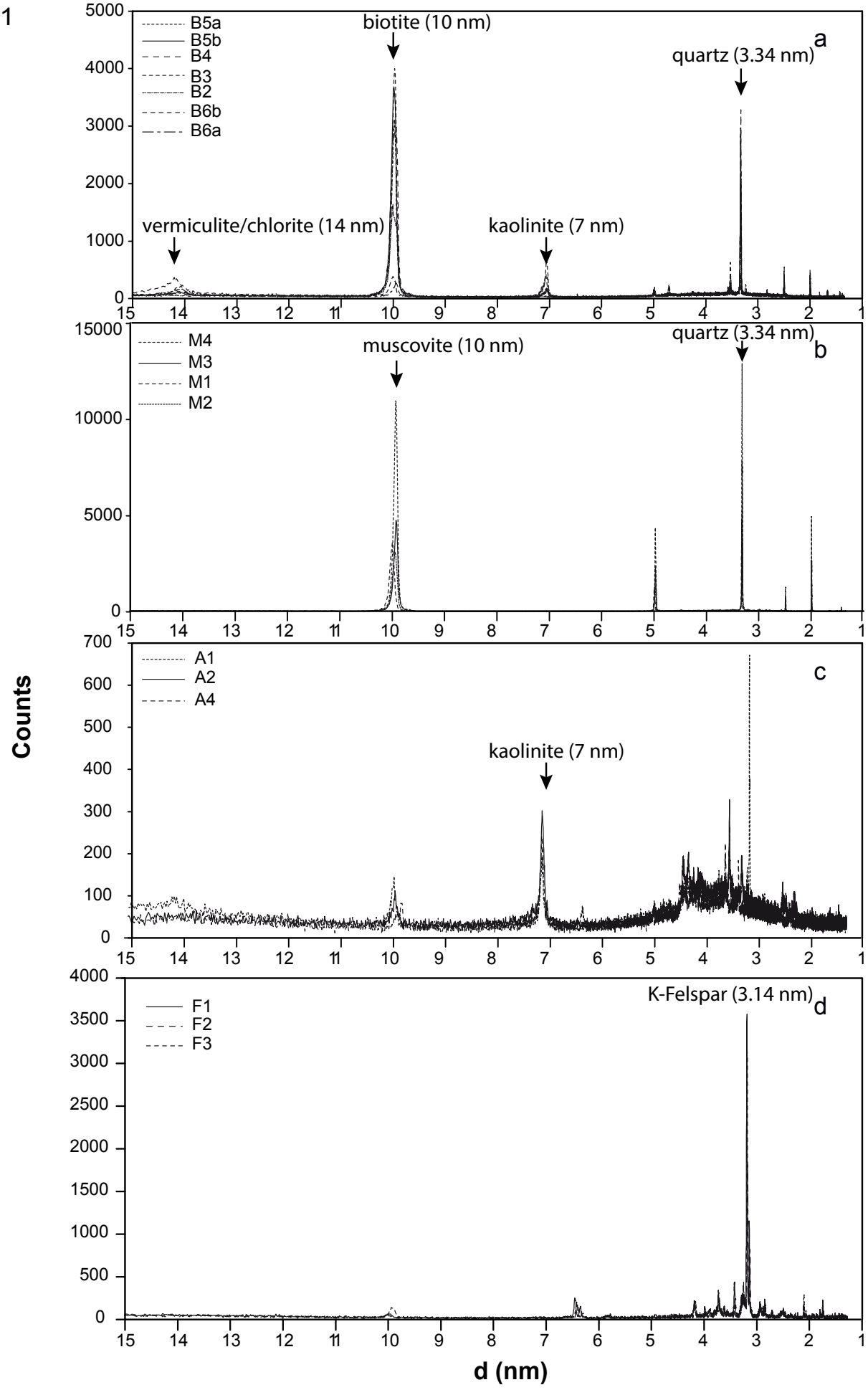
B5a
B5b
B4
B3
B2
B6b
B6a
biotite (10 nm)
quartz (3.34 nm)
a
vermiculite/chlorite (14 nm)
kaolinite (7 nm)
M4
M3
M1
M2
muscovite (10 nm)
quartz (3.34 nm)
b
A1
A2
A4
c
kaolinite (7 nm)
F1
F2
F3
K-Felspar (3.14 nm)
d
Counts
d (nm)

figure A2

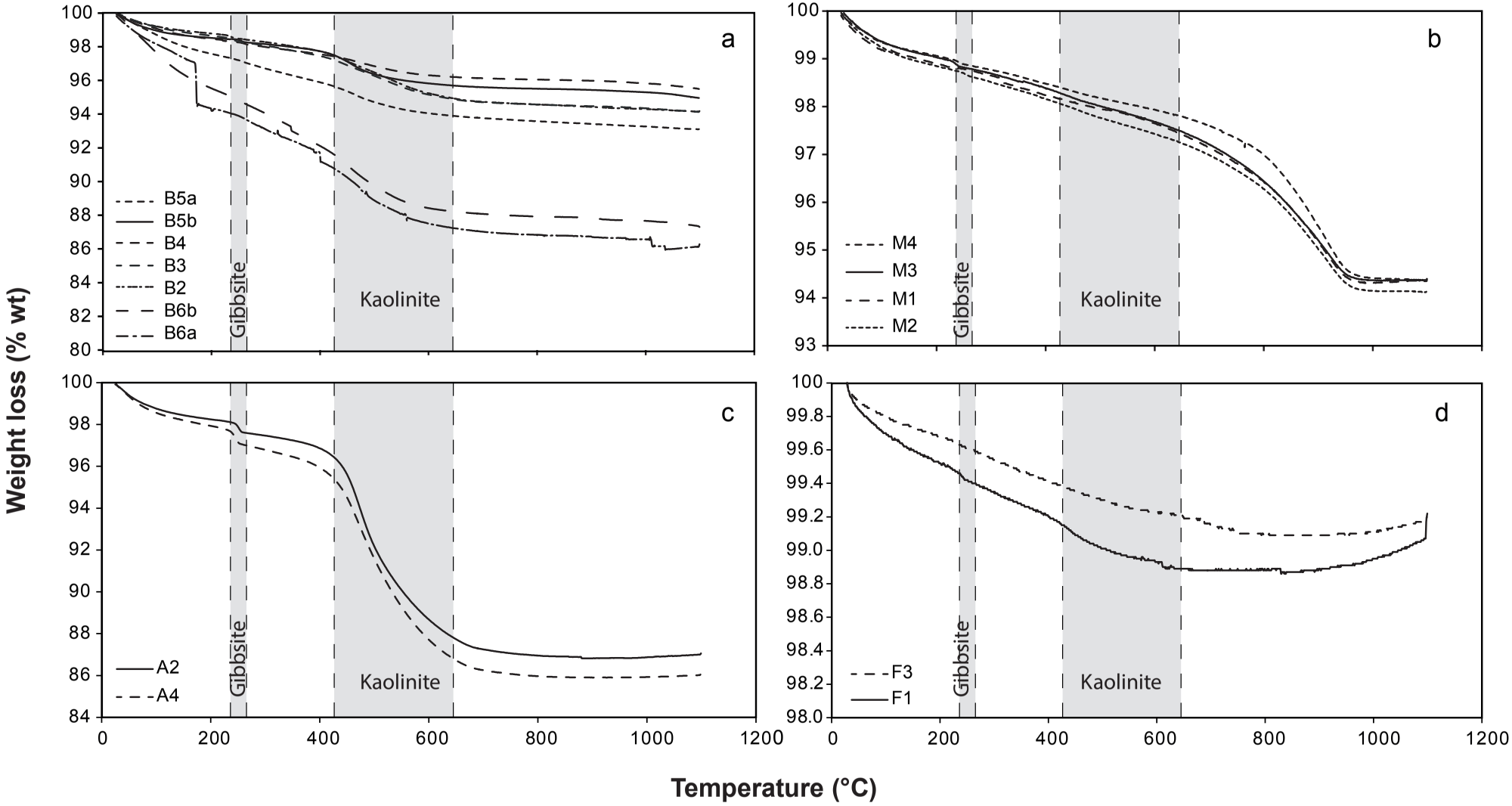
a
b
c
d
B5a
B5b
B4
B3
B2
B6b
B6a
M4
M3
M1
M2
A2
A4
F3
F1
Gibbsite
Kaolinite
Weight loss (% wt)
Temperature (°C)

Table 1: Composition of primary and secondary minerals from well-preserved and weathered granite samples determined by microprobe analyses on granite or soil thin sections (Mareschal, 2008; Mareschal et al., 2015). Gibbsite and hematite are taken from Deer et al., 1996.

	SiO_2	Al_2O_3	FeO[1]	CaO	MgO	K_2O	Na_2O	MnO	TiO_2	Total
Biotites	34.9	18.4	22.2	<DL[2]	3.8	9.2	0.25	0.62	3.5	93.2
STD (1 σ)	*0.7*	*1.5*	*0.7*		*0.3*	*0.3*	*0.07*	*0.15*	*1.1*	-
Muscovites	46.0	32.2	2.45	<DL[2]	1.03	10.4	0.70	<DL[2]	0.12	93.0
STD (1 σ)	*1.3*	*1.6*	*0.56*		*0.32*	*0.4*	*0.19*		*0.09*	-
K-feldspar	64.3	18.1	<DL[2]	<DL[2]	<DL[2]	15.5	0.88	<DL[2]	<DL[2]	99.0
STD (1 σ)	*0.4*	*0.4*				*0.96*	*0.59*			-
Albite	66.4	20.7	<DL[2]	1.38	<DL[2]	0.57	10.5	<DL[2]	<DL[2]	99.6
STD (1 σ)	*0.4*	*0.3*		*0.23*		*0.17*	*0.3*			-
Kaolinite	45.0	39.5	1.00	<DL[2]	0.06	0.08	0.10	<DL[2]	0.20	86.6
STD (1 σ)	*1.1*	*0.99*	*0.02*		*0.01*	*0.02*	*0.01*		*0.02*	-
Vermiculite	49.0	33.6	1.70	<DL[2]	1.09	1.47	0.08	0.11	0.14	87.2
STD (1 σ)	*1.1*	*0.8*	*0.02*		*0.02*	*0.76*	*0.01*	*0.01*	*0.02*	-
Hematite	-	-	96.0	-	-	-	-	-	-	96.0
STD (1 σ)	-	-	-	-	-	-	-	-	-	-
Gibbsite	-	65.4	-	-	-	-	-	-	-	65.4
STD (1 σ)	-	-	-	-	-	-	-	-	-	-

[1]Total Fe (FeO + Fe_2O_3)
[2]Below detection microprobe limit (DL)

Table 2: Boron concentration and isotopic composition of pore and bound waters.

	[B] (ng B/ mL)	$\delta^{11}B$ (‰)	Water/rock ratio (L/kg)
20-30 cm horizon pore water	12.0	30.3	0.003
20-30 cm horizon bound water	8.4	22.3	0.025
110-140 cm horizon pore water	-	-	0
110-140 cm horizon bound water	12.5	18.9	0.013

Table 3: Mineral phases identified in each sample using a combination of XRD, SEM and differential thermal analyses (Figure A1). These phases were then used for quantitative mineralogy calculations (Eq. 3 in text)

Samples	Identified mineral phases
Biotite	Biotite, kaolinite, vermiculite, titanium oxides, quartz, gibbsite, chlorite[1]
Muscovites	Muscovite, K-feldspar, quartz
K-feldspar	K-feldspar
Albite	Albite, kaolinite, gibbsite, muscovite, quartz, hematite[2]

[1]Samples B0b, B5a, B5b and B6a only
[2]Sample AH only

Table 4: Major elements, B concentration and B isotopic composition in all studied samples (see table 3 for abbreviations).

	Primary mineral	Depth (cm)	SiO_2	Al_2O_3	MgO	CaO	Fe_2O_3	MnO	TiO2	Na_2O	K_2O	$\delta^{11}B$ (‰)	B ($\mu g.g^{-1}$)	1
DL[1]			*0.009*	*0.002*	*0.0007*	*0.002*	*0.002*	*0.003*	*0.00003*	*0.01*	*0.004*	*+/-0.6*	*0.7*	
A1	*Albite*	G.B.[3]	67.1	18.7	0.7	0.3	0.1	0.02	0.01	5.8	0.2	-24.7	86.2	
A2		130-140	48.9	33.8	0.4	<DL	0.6	<DL	<DL	0.2	2.1	-16.1	108.6	
A3		120-130	47.2	35	0.4	<DL	0.6	<DL	<DL	0.2	1.9	-17.2	160	
A4		110-120	47.8	35.1	0.5	0.1	0.6	<DL	0.1	0.1	2	-15.4	185.2	
AH		130-140	43.8	33.6	0.6	<DL	5.7	0.1	<DL	0.8	1.6	-27.9	471.8	
B0a	*Biotite*	G.B.[3]	42.4	19.7	7.1	<DL	16.9	0.3	1.8	1.2	5.4	-31.1	21	
B0b		G.B.[3]	43	18.9	4.2	0.1	19	0.5	2.4	0.7	7.2	-26.8	74.2	
B1		G.B.[3]	41.7	21.4	4.3	0.1	15.3	0.5	2.2	0.6	5.5	-19.4	17.5	
B2		130-140	42.3	20.2	4.8	<DL	15.5	0.4	2.9	0.3	4.2	-16.4	7.2	
B3		120-130	44.1	20.2	4.8	<DL	16.1	0.5	2.6	0.3	4.4	-21.5	7.7	

B4		110-120	41.1	19.9	5.5	<DL	18.7	0.5	3.3	0.3	5	-16.1	3.4	
B5a		20-30	43.3	19.9	4.1	0.1	18.1	0.5	2.5	0.6	6.3	-23.5	81	
B5b		20-30	43.5	20.8	4.1	0.1	17.1	0.5	2.7	0.4	5.4	-23	34.5	
B6a		20-30	34.8	21.7	5.7	0.1	22.7	0.7	1.4	0.2	2.6	-16.3	1.3	
B6b		20-30	39.5	20.8	3.4	0.1	19	0.8	1.3	0.5	2.4	-16.2	0.9	
F1	*K-Felsdpar*	G.B.[3]	64.6	18.2	<DL	0.2	0.2	<DL	<DL	3.3	11.4	-30.2	6.3	
F2		130-140	64.7	18.2	0.1	0.1	0.2	<DL	<DL	2.7	12.1	-30.8	10.7	
F3		120-130	64	18.3	0.1	0.1	0.3	<DL	<DL	2.6	12.2	-31.2	11.5	
F4		110-120	62.7	18.4	0.1	0.1	0.5	<DL	<DL	2.1	12.7	-33.1	10.2	
M1	*Muscovite*	G.B.[3].	44.8	31.3	1.3	0.1	3.4	0.1	0.1	0.9	9.5	-30.7	76.1	
M2		130-140	44.3	31.2	1.4	<DL	3	0.1	0.1	1	9.5	-21.4	78.3	
M3		120-130	45.3	31.4	1.4	<DL	3.1	0.1	0.1	0.8	9.4	-23.8	89.5	
M4		110-120	45.7	32.1	1.3	<DL	3.1	0.1	0.1	0.7	9.7	-19.4	22.5	

[1]Detection limit for all elements (except for boron isotopic composition where measurement external reproducibility is given).

[2]Loss on ignition

[3]Unaltered granite